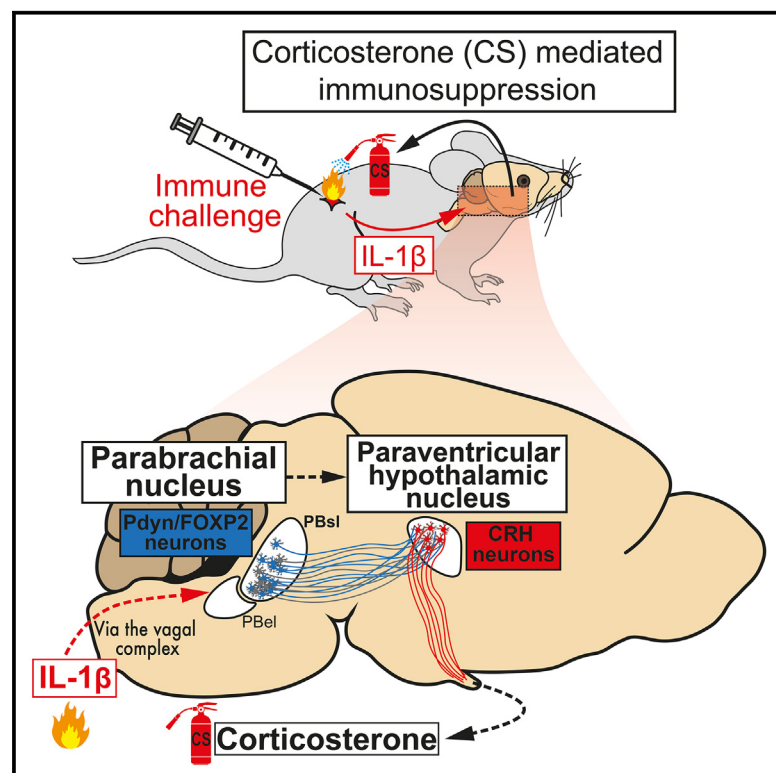


# The parabrachial nucleus elicits a vigorous corticosterone feedback response to the pro-inflammatory cytokine IL-1 $\beta$

## Graphical abstract



## Authors

Ferdinand Jagot,  
Romane Gaston-Breton,  
Ana Jeemin Choi, ...,  
Pierre-Marie Lledo, Gabriel Lepousez,  
G rard Eberl

## Correspondence

ferdinandjagot@gmail.com (F.J.),  
gerard.eberl@pasteur.fr (G.E.)

## In brief

Jagot et al. identify a brainstem-to-hypothalamus neuronal circuit in mice by which the cytokine IL-1 $\beta$  induces the corticosterone response and mediates immunosuppression.

## Highlights

- IL-1 $\beta$  and TNF- $\alpha$  trigger vigorous corticosterone release in mice
- IL-1 $\beta$  recruits a parabrachial to the paraventricular hypothalamic nucleus circuit
- The vagal complex activates PB-to-PVN neurons to induce the corticosterone response
- Reactivation of IL-1 $\beta$ -activated parabrachial neurons induces immunosuppression



## Article

# The parabrachial nucleus elicits a vigorous corticosterone feedback response to the pro-inflammatory cytokine IL-1 $\beta$

Ferdinand Jagot,<sup>1,2,3,\*</sup> Romane Gaston-Breton,<sup>1</sup> Ana Jeemin Choi,<sup>1,3</sup> Maud Pascal,<sup>1,2</sup> Lena Bourhy,<sup>2</sup> Romane Dorado-Doncel,<sup>1</sup> Karl-Klaus Conzelmann,<sup>4</sup> Pierre-Marie Lledo,<sup>2,5</sup> Gabriel Lepousez,<sup>2,5</sup> and Gérard Eberl<sup>1,5,6,\*</sup>

<sup>1</sup>Institut Pasteur, Université de Paris Cité, Inserm U1224, Microenvironment and Immunity Unit, 75015 Paris, France

<sup>2</sup>Institut Pasteur, Université de Paris Cité, CNRS UMR 3571, Perception and Memory Unit, 75015 Paris, France

<sup>3</sup>PhD Program, Ecole Doctorale Bio Sorbonne Paris Cité (BioSpc), Université de Paris Cité, 75005 Paris, France

<sup>4</sup>Max von Pettenkofer Institute of Virology, Medical Faculty and Gene Center, LMU Munich, 81377 Munich, Germany

<sup>5</sup>These authors contributed equally

<sup>6</sup>Lead contact

\*Correspondence: [ferdinandjagot@gmail.com](mailto:ferdinandjagot@gmail.com) (F.J.), [gerard.eberl@pasteur.fr](mailto:gerard.eberl@pasteur.fr) (G.E.)

<https://doi.org/10.1016/j.neuron.2023.05.009>

## SUMMARY

The central nervous system regulates systemic immune responses by integrating the physiological and behavioral constraints faced by an individual. Corticosterone (CS), the release of which is controlled in the hypothalamus by the paraventricular nucleus (PVN), is a potent negative regulator of immune responses. Using the mouse model, we report that the parabrachial nucleus (PB), an important hub linking interoceptive afferent information to autonomic and behavioral responses, also integrates the pro-inflammatory cytokine IL-1 $\beta$  signal to induce the CS response. A subpopulation of PB neurons, directly projecting to the PVN and receiving inputs from the vagal complex (VC), responds to IL-1 $\beta$  to drive the CS response. Pharmacogenetic reactivation of these IL-1 $\beta$ -activated PB neurons is sufficient to induce CS-mediated systemic immunosuppression. Our findings demonstrate an efficient brainstem-encoded modality for the central sensing of cytokines and the regulation of systemic immune responses.

## INTRODUCTION

In the 1920s, Metalnikov observed that conditioned neural reflexes modulate immune responses to antigens.<sup>1</sup> Decades later, it was found that bacterial compounds, such as lipopolysaccharides (LPS) and the pro-inflammatory cytokine responses they elicit, such as interleukin-1 $\beta$  (IL-1 $\beta$ ) and tumor necrosis factor alpha (TNF- $\alpha$ ), induce a vigorous and complex response coordinated by the brain.<sup>2</sup> Referred to as “sickness behavior,” this response promotes behavioral changes (e.g., reduced locomotion and food intake, social avoidance), metabolic adjustments (e.g., fever, glycemia), and autonomic or neuroendocrine responses in ways that increase individual and social resistance to infection and, at the same time, regulate immune responses to prevent runaway responses and shock. Recent studies show that infection-induced behavioral and temperature adjustments are controlled by neurons in the brainstem<sup>3</sup> and the hypothalamus,<sup>4</sup> respectively. Furthermore, neurons in the insular cortex can activate the immune system and trigger inflammation.<sup>5</sup> However, the identity of the neurons involved in the regulation of the immune system upon infection remains unclear.

The brain regulates immune responses mainly through the autonomic and neuroendocrine systems. Autonomic responses,

conveyed by the sympathetic and the parasympathetic nervous systems, are initiated by preganglionic brain neurons and induce the release by terminal neurons of neurotransmitters, neuropeptides, and neurohormones that modulate immunity. Cortisol (or corticosterone, CS, in mice) is released into the bloodstream and efficiently suppresses immune responses to limit immunopathology and mobilize energy for other activities.<sup>6</sup> The primary inducer of the CS response is the paraventricular nucleus (PVN) of the hypothalamus. In the PVN, neurons expressing corticotropin-releasing hormone (CRH) and vasopressin (VP) initiate the hypothalamo-pituitary-adrenal (HPA) cascade, leading to CS production by the adrenal gland.<sup>7</sup> Importantly, the activity of PVN neurons—and, therefore, the kinetics and amplitude of the CS response—depends on the integration of signals received from other brain regions, as well as from circumventricular organs that monitor the blood, such as the area postrema (AP).<sup>8</sup>

The CS response is strongly induced by psychological, sensory (pain)-, and immune “stress” signals. In the context of exposure to the microbial compound LPS or the pro-inflammatory cytokine IL-1 $\beta$ , a direct excitatory input from catecholaminergic neurons in the nucleus of the solitary tract (NTS) and the rostral ventral medulla (RVM) of the brainstem has been shown to



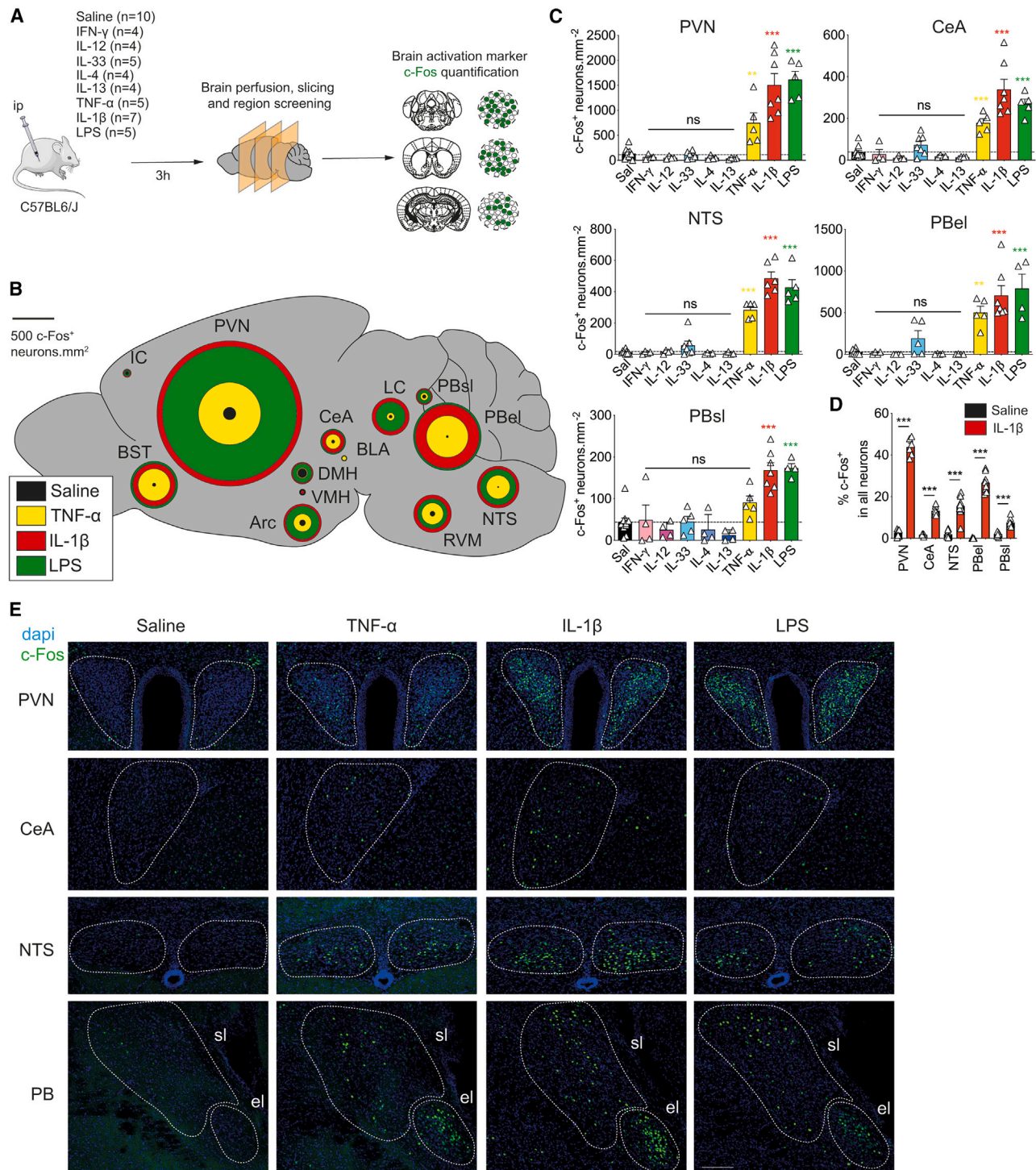


**Figure 1. Systemic cytokines selectively activate a complex neuronal circuit**

(A) C57BL6/J mice were injected into the peritoneum with cytokines or LPS and assessed for c-Fos expression in brain sections. The number of mice is indicated for each cytokine (n), corresponding to the mean of c-fos counts of both brain hemispheres for each brain region.

(B) Quantitative mapping of c-Fos expression following treatment. The diameter of circles is proportional to the density of c-Fos<sup>+</sup> neurons. Arc: arcuate nucleus. BLA: basolateral amygdala. BST: bed nucleus of the stria terminalis. CeA: central amygdala. DMH: dorsomedial hypothalamus IC: insular cortex. LC: Locus coeruleus. NTS: nucleus of the tractus solitarius. PBsl: parabrachial nucleus, latero-superior zone. PBel: parabrachial nucleus, latero-external zone. PVN: paraventricular nucleus. RVM: rostro-ventral medulla. VMH: ventromedial hypothalamus.

(legend continued on next page)



provide one pathway initiating the CS response.<sup>9</sup> However, additional excitatory neurons regulate the activity of the PVN from the forebrain regions, such as the lateral septum, the bed nucleus of the stria terminalis (BST), and the central amygdala (CeA), and brainstem regions, such as the parabrachial nucleus (PB).<sup>10,11</sup> The PB is a major hub connecting interoceptive afferent information from spinal neurons<sup>12</sup> and the vagal complex (VC)<sup>13</sup> to various autonomic outputs and aversive behaviors through the CeA-BST network and nocifensive behaviors through various projections to the reticular formation, the ventromedial hypothalamus (VMH), and the intralaminar thalamic nuclei.<sup>12,14,15</sup> Despite this anatomical knowledge, we still have limited information about the nature of the peripheral immune signals perceived by the brain, the detection site of immune signals, and the neuronal circuit capable of regulating systemic immune responses.

To unravel the brain regions and their underlying circuits, which relay the sensing of pro-inflammatory cytokines to the PVN and induce the CS response, we administered different types of cytokines and mapped the activated brain areas at cellular resolution using c-Fos staining. The strongest brain responses were observed in response to the cytokines IL-1 $\beta$  and TNF- $\alpha$  and were accompanied by a vigorous CS response. Using genetic tagging methods combined with viral tracing, we found the PB to be a major hub linking the sensing of IL-1 $\beta$  with the activation of the CS response in the PVN. Furthermore, we demonstrated that activation of PB neurons was sufficient—but not necessary—to trigger a vigorous CS response via efferents to the PVN, ultimately leading to immunosuppression. Our data delineate a novel dedicated brain circuit that prevents potentially damaging systemic inflammation and maintains homeostasis.

## RESULTS

### Anti-microbial cytokines activate brain nuclei associated with peripheral sensing, sickness behavior, and CS response

To obtain a whole-brain map of neurons and regions responsive to different immune signals that encompass the three major types of effector immunity, we injected mice into the peritoneum with cytokines mediating anti-viral type-1 responses (IFN- $\gamma$  and IL-12), anti-helminth and pro-repair type-2 responses (IL-33, IL-4, and IL-13), or anti-microbial (bacteria and fungi) type-3 responses (TNF- $\alpha$  and IL-1 $\beta$ ), as well as with LPS, a bacteria-derived and strong inducer of type-3 responses (Figure 1A). After 3 h, brains were prepared for c-Fos staining, an early marker of neuronal activation,<sup>16</sup> and imaged in serial sections. Our broad screen revealed major differences in the activation pattern of neurons by the different types of cytokines. Although IFN- $\gamma$ , IL-12, IL-33, IL-4, and IL-13 did not induce significant c-Fos

expression, TNF- $\alpha$ , IL-1 $\beta$ , and LPS markedly increased expression of c-Fos in numerous brain regions (Figures 1B–1E, S1A, and S1B). In particular, TNF- $\alpha$ , IL-1 $\beta$ , and LPS induced the activation of neurons in brainstem areas integrating visceral sensory inputs, such as the NTS and PB, regions involved in sickness and defensive behavior such as the CeA and BST, as well as hypothalamic regions involved in metabolic homeostasis and food intake such as the arcuate nucleus (Arc) and the dorsomedial hypothalamus (DMH) (Figures 1B, S1A, and S1B).<sup>17</sup> In some activated regions, TNF- $\alpha$ , IL-1 $\beta$ , and LPS induced the activation of specific neuronal subpopulations, such as catecholaminergic neurons in the locus coeruleus (LC) and RVM, calcitonin G-related peptide (CGRP)<sup>+</sup> neurons in the PB, as well as protein kinase C (PKC)- $\delta$ <sup>+</sup> neurons in the CeA and the BST (Figures S1C–S1H). These brain regions are involved in alertness, food intake, defensive behaviors, and autonomic responses such as the CS response.<sup>18–22</sup> Of note, the absence of response to some cytokines and saline ruled out an effect of stress alone associated with injection (Figure 1C).

The highest density of neurons activated by TNF- $\alpha$ , IL-1 $\beta$ , and LPS was observed in the PVN (Figures 1B and 1D). In this region, IL-1 $\beta$  recruited up to 43.8%  $\pm$  2.1% of the total PVN cells (Figure 1D). As the PVN triggers the HPA axis for the release of CS into the bloodstream, we quantified the robustness of the cytokines-induced PVN activation by measuring CS level. In agreement with their respective c-Fos activation profiles, TNF- $\alpha$ , IL-1 $\beta$ , and LPS effectively induced a CS response, whereas other cytokines were inefficient (relative to saline; Figure 2A). Furthermore, double immunostaining showed that IL-1 $\beta$  activated a large proportion of CRH-expressing neurons (97.7%  $\pm$  2%) and almost half of VP-expressing neurons (43.0%  $\pm$  6%) in the PVN (Figures 2B–2D), which synergize to activate the HPA cascade and the CS response.<sup>7</sup> We observed that the CS response to IL-1 $\beta$  was higher in females than in males, in accordance with previous data showing their increased sensitivity to stress (Figure S1I).<sup>23</sup> Interestingly, increasing doses of IL-1 $\beta$  did not increase the levels of CS in the blood but rather prolonged the duration of the CS response (Figures 2E and S1J). Finally, as inflammation-dependent changes in the reactivity of the HPA axis were reported at the neurohormonal level,<sup>24</sup> we assessed whether repeated injections of IL-1 $\beta$  would alter the profile of the CS response and we found that re-injection of IL-1 $\beta$  did not alter the kinetic and amplitude of the CS response (Figures 2F and S1K).

Altogether, these results demonstrate that immune responses induced by LPS and mediated by IL-1 $\beta$  and TNF- $\alpha$ , but not prototypical cytokines mediating type-1 or type-2 immune responses, are potent activators of brain circuits involved in the management of defensive and sickness behavior and promptly activate the CS response.

(C) Density of c-Fos<sup>+</sup> neurons in individual brain regions. Dotted lines indicate the mean obtained in the saline-injected group (Sal). Data are mean  $\pm$  SEM. One-way ANOVA, ns = not significant, \* $p$  < 0.05, \*\* $p$  < 0.01, \*\*\* $p$  < 0.001 compared with saline. See Table S1 for statistics.

(D) Proportion of c-Fos<sup>+</sup> neurons among all DAPI<sup>+</sup> neurons in the PVN, CeA, NTS, PBel and PBsl, and after IL-1 $\beta$  injection (versus saline control). Data are mean  $\pm$  SEM ( $n$  = 8–12).  $t$  test, ns = not significant, \* $p$  < 0.05, \*\* $p$  < 0.01, and \*\*\* $p$  < 0.001 compared with saline. See Table S1 for statistics.

(E) Representative images of c-Fos expression by immunofluorescence. Scale bar is 200  $\mu$ m.

Results are representative of 3 independent experiments pulled together.



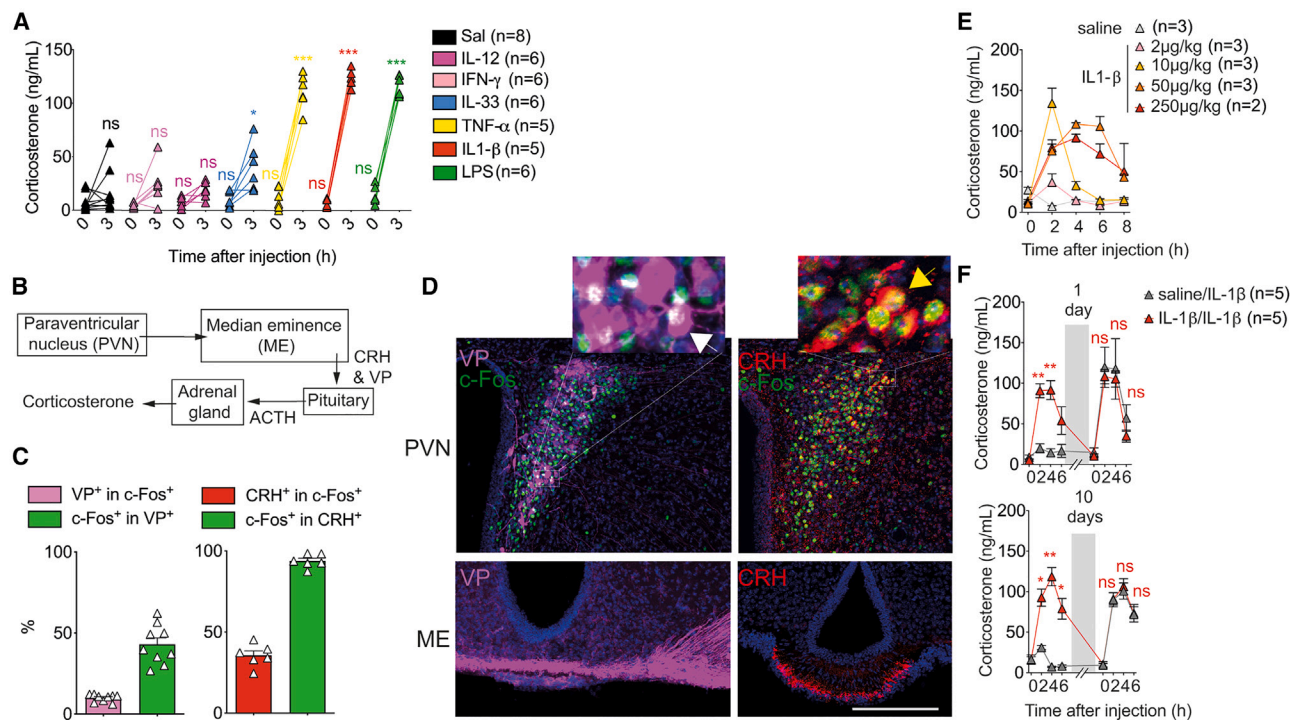


**Figure 2. IL-1 $\beta$  efficiently induces a dose-dependent corticosterone response**

(A) Blood corticosterone (CS) levels immediately before (0 h) or 3 h after cytokine or LPS injection into the peritoneum. Data are mean  $\pm$  SEM; two-way ANOVA, ns = not significant, \* $p$  < 0.05, \*\* $p$  < 0.01, \*\*\* $p$  < 0.001 compared with saline. See Table S1 for statistics.

(B) Brain regions and mediators of the hypothalamo-pituitary axis (HPA) leading to CS release into the bloodstream. CRH: corticotropin-releasing hormone. VP: vasopressin.

(C) Proportion of IL-1 $\beta$ -induced c-Fos $^{+}$  neurons expressing vasopressin (VP, pink) or corticotropin-releasing hormone (CRH, red), and conversely, the proportion of VP $^{+}$  (green, left) or CRH $^{+}$  (green, right) neurons expressing IL-1 $\beta$ -induced c-Fos (n = 6 mice for VP and 3 mice for CRH).

(D) Representative images of c-Fos colocalization with VP $^{+}$  and CRH $^{+}$  neurons within the PVN (upper images), and projection of VP and CRH fibers into the ME (lower images), 3 h after IL-1 $\beta$  injection. White and yellow arrows show c-Fos $^{+}$ VP $^{+}$  and c-Fos $^{+}$ CRH $^{+}$  neurons, respectively. Scale bar is 200  $\mu$ m.

(E) Dose-dependent effect of IL-1 $\beta$  injection on the blood CS response. One of two independent experiments (replicate experiment shown in Figure S2).

(F) CS response after re-injection of IL-1 $\beta$  1 day (left) or 10 days (right) after initial injection. Data are mean  $\pm$  SEM; two-way ANOVA, ns = not significant, \* $p$  < 0.05, \*\* $p$  < 0.01, \*\*\* $p$  < 0.001 compared with saline. One of two independent experiments (replicate experiment shown in Figure S2). See Table S1 for statistics.

### A subpopulation of PB neurons directly induces the CS response

To decipher the circuits linking the activation of PVN neurons with the integration of peripheral cytokine signals, we examined whether brain regions activated by IL-1 $\beta$  (the strongest activator of the PVN, Figure 1B) include neurons projecting to the PVN. Following adeno-associated virus (AAV)-based retrograde tracing from the PVN, we analyzed the density of retrogradely labeled cells in the brain regions activated by IL-1 $\beta$  (Figure 1B). As expected from previous work, we observed a high density of PVN-projecting neurons in the NTS, LC/pre-LC, Arc, and PB (Figures 3A and 3B). The PB, a major hub connecting interoceptive afferent information from spinal neurons<sup>12</sup> and the VC<sup>13</sup> to various autonomic outputs, was strongly recruited after IL-1 $\beta$  injection. Different types of PB neurons have been identified, according to their neurochemical markers and projection patterns. For instance, CGRP $^{+}$  neurons in the external part of the lateral PB (PBel) project to the BST and CeA and initiate fear and satiety behaviors,<sup>25</sup> whereas FoxP2 $^{+}$  PBsl neurons project preferentially to the hypothalamus.<sup>26</sup> In order to identify the PB neurons that acti-

vate the PVN and induce the CS response, we used dual stereotaxic injections of Cre-expressing retrograde AAVs combined with Cre-dependent AAVs expressing the fluorescent reporter mCherry to identify PB neurons that project to PVN (PB-to-PVN neurons; Figures 3C–3E). As a comparison, we labeled PB neurons projecting to BST (PB-to-BST neurons) or CeA (PB-to-CeA neurons), both known to control behavioral responses to threat and pain.<sup>25</sup> PB-to-PVN neurons were mostly found within the PBsl, whereas PB-to-CeA and PB-to-BST neurons were also found within the PBel (Figures 3D and 3E). In accordance with the reported projection profile of CGRP $^{+}$  neurons in the PBel,<sup>25</sup> PB-to-CeA, and PB-to-BST neurons, but not PB-to-PVN neurons, projected to both BST and CeA (Figures 3D and 3E). We then used Cre-dependent AAVs expressing the hM3D(Gq) receptor (a Designer Receptor Exclusively Activated by Designer Drug [DREADDs]) to pharmacogenetically manipulate PB neurons (Figures 3F and 3G). After injection of the ligand clozapine N-oxide (CNO) to selectively activate the hM3D(Gq)-expressing neurons (compared with mCherry-injected control), we found that only PB-to-PVN

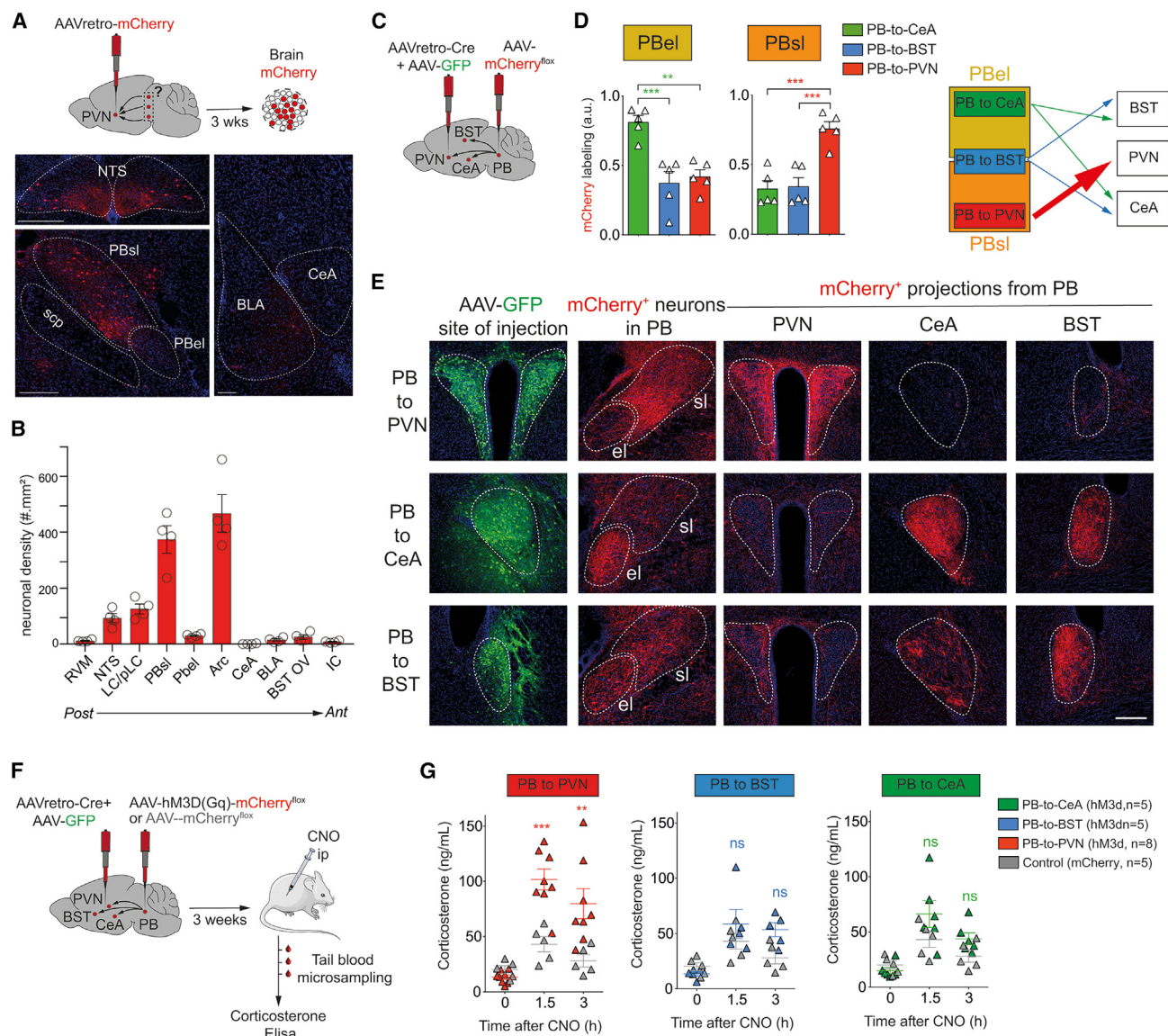


**Figure 3. PB neurons directly induce the corticosterone response by projecting to the PVN**

(A) Top, viral tracing strategy to retrolabel the neurons projecting to the PVN. Bottom, representative images of retrogradely labeled neurons. Scale bar: 200  $\mu$ m. (B) Quantification of the density of retrogradely labeled neurons in selected brain regions known to be activated by IL-1 $\beta$  (see Figure 1B;  $n = 4$  mice). (C) Viral strategy for selective tracing of PB neurons projecting to the PVN, BST, or CeA. (D) Quantification of mCherry<sup>+</sup> labeling intensity in the Pbel and PBsl. Data are mean  $\pm$  SEM. One-way ANOVA ( $n = 5$  mice per group), ns = not significant, \* $p < 0.05$ , \*\* $p < 0.01$ , \*\*\* $p < 0.001$  compared with control. See Table S1 for statistics. (E) Representative images of the site of Cre virus injection (AAV-GFP) and of mCherry<sup>+</sup> neuron projections to the PVN, BST, and CeA. Scale bar is 200  $\mu$ m. (F) Viral strategy for DREADD-based restimulation of PB neurons projecting to the PVN, BST, or CeA. (G) Blood levels of CS after activation of PB-to-CeA, PB-to-BST, or PB-to-PVN neurons. Control individuals were injected with AAVretro-Cre into the PVN and mCherry<sup>lox</sup> control virus into the PB. Data are mean  $\pm$  SEM. Two-way ANOVA ( $n = 5$ –8 mice per group), ns = not significant, \* $p < 0.05$ , \*\* $p < 0.01$ , and \*\*\* $p < 0.001$  compared with control. See Table S1 for statistics.

neurons triggered a significant CS response (Figure 3G). We concluded that a subpopulation of neurons in the PBsl sends axonal projections to the PVN and induces the CS response.

### PB-to-PVN neurons respond to IL-1 $\beta$

To confirm that PB-to-PVN neurons in the PBsl are recruited by IL-1 $\beta$ , we performed *in vivo* fiber photometry recording of the ac-

tivity of PB-to-PVN neurons in response to peripheral injection of IL-1 $\beta$ . The calcium-sensitive activity reporter GCaMP7f was conditionally expressed in PB-to-PVN neurons. The bulk fluorescence was collected in freely moving animals using an optic fiber implanted above the PBsl (Figures 4A and 4B), resulting in spontaneous calcium-dependent fluorescence fluctuations—a proxy for synchronous population activity.<sup>27,28</sup> At baseline, the

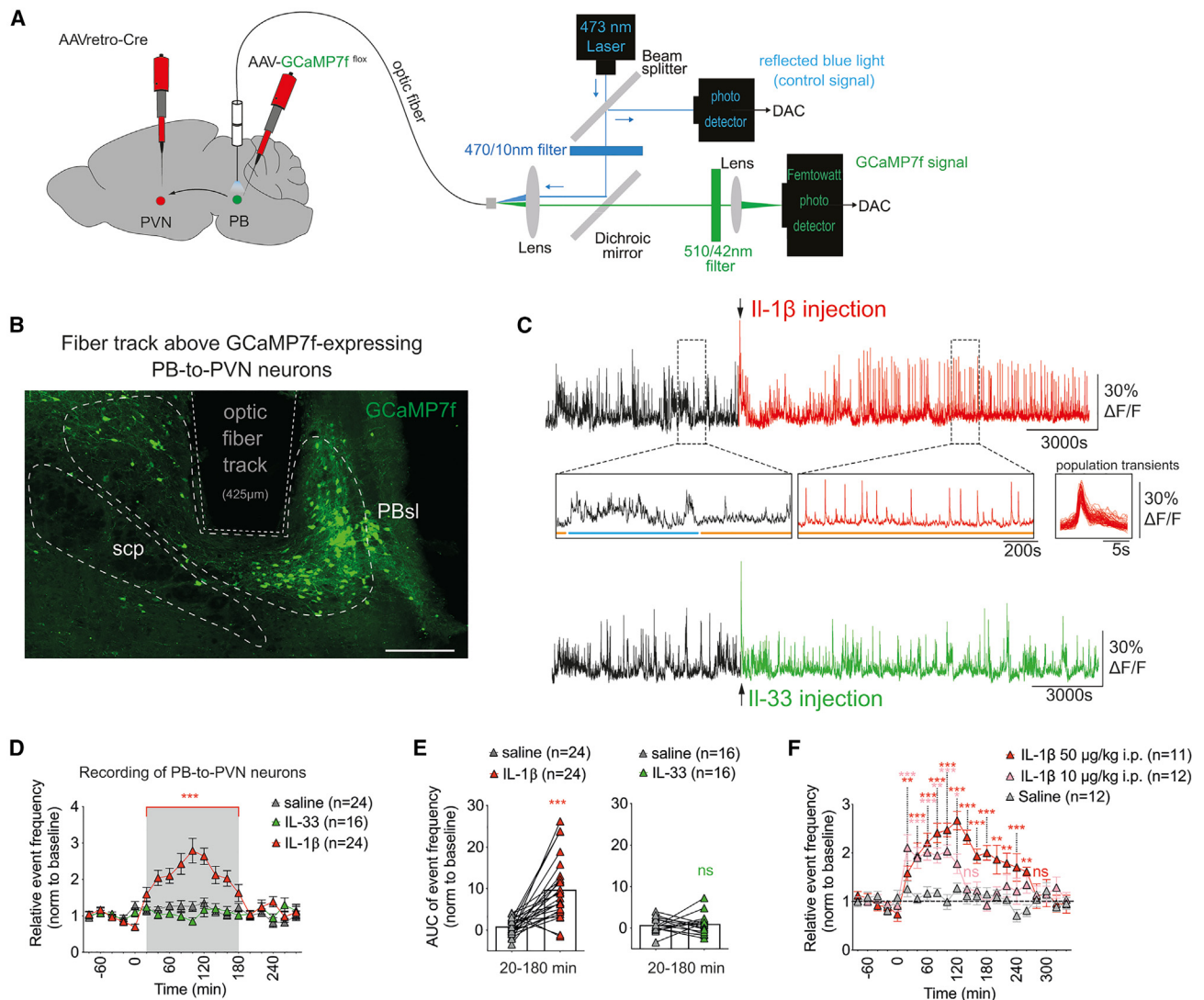


**Figure 4. IL-1 $\beta$  activates the PB-to-PVN neurons**

(A) PB-to-PVN neurons were conditionally labeled with a Gcamp7f calcium reporter using a dual viral strategy and recorded through an optical fiber (425  $\mu$ m) chronically implanted above the PBsl.

(B) Representative image of the fiber track recording GCaMP7f-expressing PB-to-PVN neurons. Scale bar is 200  $\mu$ m.

(C) Representative photometry bulk fluorescence signals of the PB-to-PVN neuronal population before and after IL-1 $\beta$  or IL-33 intraperitoneal injection. Note the acute increase of activity following hand restrain. Higher magnifications of the fluorescence signal before and after IL-1 $\beta$  show the baseline changes in population activity dynamics with behavioral state (active exploration, blue; immobility, orange) and the IL-1 $\beta$ -induced emergence of regular, stereotyped, large-amplitude population transients during the sickness phase. Right, overdrawn sorted population events observed following IL-1 $\beta$  injection.

(D) Changes in the PB-to-PVN population transients frequency after saline, IL-1 $\beta$ , or IL-33 injection. Data are mean  $\pm$  SEM. Two-way ANOVA (n represent single-recorded brain hemispheres), ns = not significant, \* $p$  < 0.05, \*\* $p$  < 0.01, and \*\*\* $p$  < 0.001 compared with saline. See Table S1 for statistics.

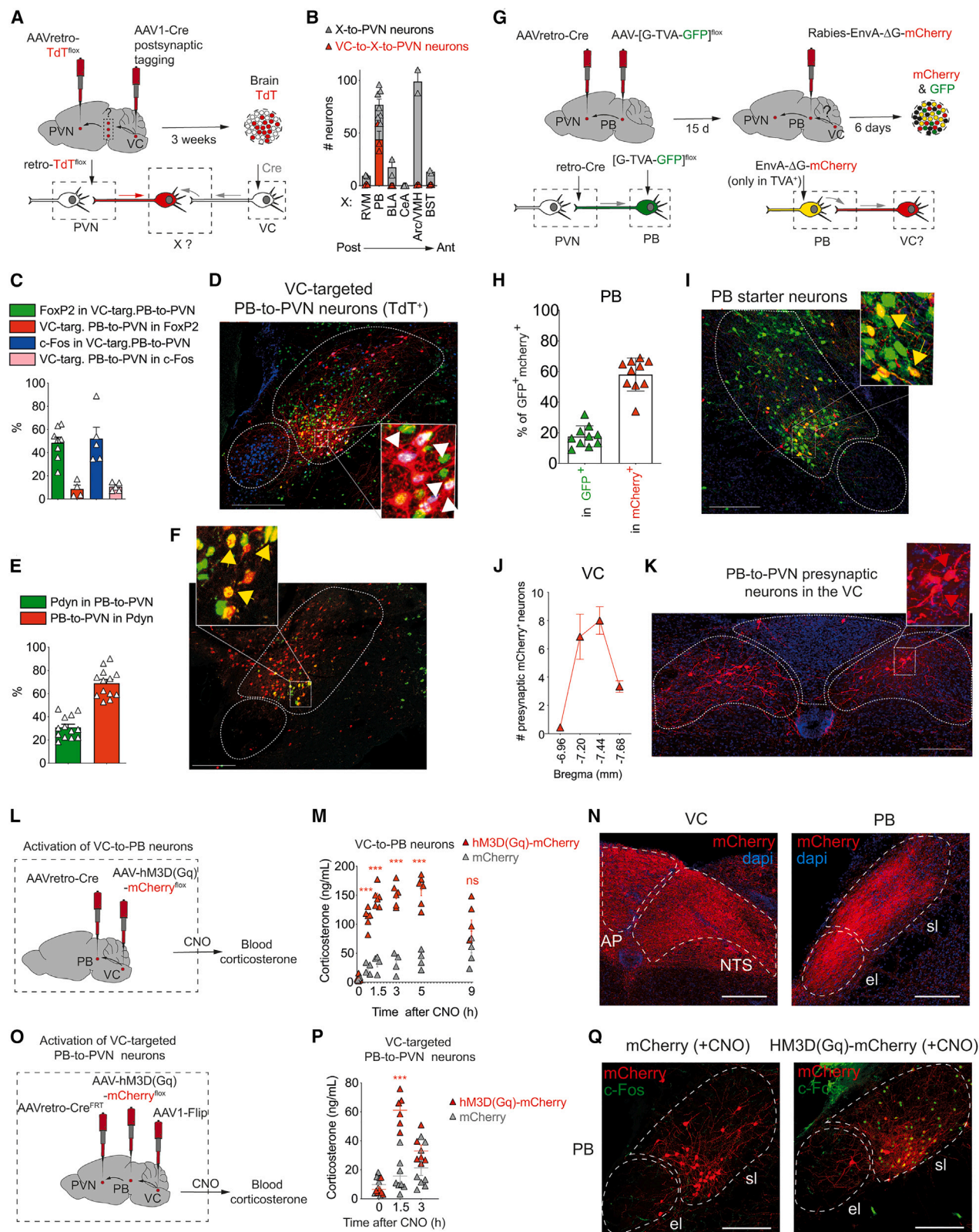
(E) Area under the curve (AUC) of the integrated PB-to-PVN population transient frequency from 20 to 180 min post-injection of IL-1 $\beta$  (left) or IL-33 (right). Data are mean  $\pm$  SEM, t test, ns = not significant, \* $p$  < 0.05, \*\* $p$  < 0.01, and \*\*\* $p$  < 0.001 compared with saline. See Table S1 for statistics.

(F) Changes in PB-to-PVN population transients frequency induced by intraperitoneal injection of IL-1 $\beta$  at 10 or 50  $\mu$ g/kg. Data are mean  $\pm$  SEM. Two-way ANOVA, ns = not significant, \* $p$  < 0.05, \*\* $p$  < 0.01, and \*\*\* $p$  < 0.001 compared with saline. See Table S1 for statistics.

PB-to-PVN neurons exhibited spontaneous population transients, with bouts of increased fluorescence associated with a high frequency of population transients during alert exploration and bouts of low fluorescence during immobility/sleep period (Figure 4C, baseline in black). The PB-to-PVN neurons also exhibited reliable time-locked population responses to stressful

events such as hand restrain and mild foot shock (Figure S2E). To control for motion artifact, we performed dual-color imaging of PB-to-PVN neurons co-expressing GCaMP7f and the Ca<sup>2+</sup>-independent fluorescent reporter mCherry (Figures S2A–S2D). mCherry traces were qualitatively different from GCaMP7f, with no noticeable fluctuation (peak mCherry  $\Delta F/F$  < 2%,





(legend on next page)

Figure S2B) and no concomitant population transients in the green and red channels during the recording time period (Figures S2B and S2C).

Upon IL-1 $\beta$  administration, we measured an initial reduction in PB activity, followed by the emergence of large, high-amplitude, regular, and stereotyped population transients (Figure 4C), reminiscent of synchronous population bursts observed upon LPS injection in CGRP<sup>+</sup> neurons of the PB,<sup>25</sup> which may originate from local network synchronization and/or synchronous external inputs.<sup>29</sup> We quantified the frequency of spontaneous population transients before and after IL-1 $\beta$  and observed that this high-activity state in the PB-to-PVN population emerged as early as 20 min after injection, reaching a peak of activity at 100 min, and lasting for 180 to 200 min (Figures 4C–4E). Higher amounts of IL-1 $\beta$  prolonged the period of sustained high activity (Figure 4F), matching the IL-1 $\beta$  dose-dependent effect on the kinetic of the CS response (Figure 2E) and suggesting that blood IL-1 $\beta$  levels are encoded into temporal activity patterns in the PB. In contrast to the strong response induced by IL-1 $\beta$ , we did not observe any effect in response to the type-2 cytokine IL-33 (Figures 4C–4E), in accordance with c-Fos quantification (Figure 1). Similarly, fasting-induced refeeding or administration of the gastric malaise-inducing agent lithium chloride had no significant effect on PB-to-PVN neuronal population activity (Figure S2F–S2H).

### The PB-to-PVN neuronal circuit is recruited by the VC

We next investigated the nature of inputs to PB-to-PVN neurons. Previous work showed that the PB receives exteroceptive sensory inputs from the periphery via the spinoparabrachial tract, as well as interoceptive vagal inputs via the NTS and the AP,<sup>12</sup> both regions belonging to the VC. We therefore investigated the contribution of those pathways in the activation of PB-to-

PVN neurons and, consequently, in the CS release in response to IL-1 $\beta$ .

First, we activated the nociceptive spinoparabrachial pathway by the subcutaneous injection of capsaicin, a ligand of heat-sensing TRPV1 channels in sensory nociceptive neurons, and assessed its impact on the activation of PB neurons (Figures S3A and S3B). Capsaicin efficiently activated PB and PVN neurons (Figure S3C), as previously reported,<sup>30</sup> and induced an early transient CS response (Figure S3D), although only poorly activating NTS and regions associated with sickness behavior, such as the BST and CeA (Figure S3C). However, despite strong c-Fos induction in the PBsl, which receives spinal inputs (Figure S3C), capsaicin neither induced significant changes in activity in the PB-to-PVN neuronal population when analyzed with fiber photometry (Figures S3E and S3F) nor induce a significant c-Fos expression in PB-to-PVN neurons (Figures S3G–S3I). Similarly, an intraperitoneal injection of capsaicin, matching the administration route of IL-1 $\beta$ , failed to activate PB-to-PVN neurons (Figure S3F). These results indicate that the TRPV1+ spinoparabrachial neurons do not participate in the activation of PB-to-PVN neurons involved in the CS response.

We next assessed whether PB-to-PVN neurons are directly activated by the VC. In order to identify PVN-projecting neurons that receive direct inputs from the VC, we injected a transsynaptic anterograde AAV1-Cre virus into the VC<sup>31</sup> and a Cre-dependent retrograde AAV expressing mCherry into the PVN (Figure 5A). PVN-projecting neurons were found in the brainstem, PB, and hypothalamus (Figures 3A and 3B). However, only the PB carried a significant number of neurons with both presynaptic contacts with VC neurons and projections to the PVN (Figure 5B, VC-to-PB-to-PVN neurons). These VC-targeted PB-to-PVN neurons were distributed along the PBsl and comprised up to

### Figure 5. Neurons in the PB relay an IL-1 $\beta$ signal from the VC to the PVN

- (A) Strategy for identifying the neuronal relay between the vagal complex (VC) and PVN neurons. AAV1-Cre virus with transsynaptic ability induces expression of Cre in post-synaptic neurons.
- (B) Quantification of neurons in brain regions directly projecting to the PVN (X-to-PVN neurons, AAVretro-mCherry into the PVN as in Figure S4,  $n = 2$ –7 mice) or VC-targeted neurons projecting to the PVN (VC-to-X-to-PVN neurons, mean  $\pm$  SEM,  $n = 3$  mice).
- (C) Proportion of VC-targeted PB-to-PVN (TdT<sup>+</sup>) neurons expressing FoxP2 (green) or IL-1 $\beta$ -induced c-Fos (blue), and conversely, the proportion of FoxP2<sup>+</sup> (dark red) or c-Fos<sup>+</sup> (light red) neurons being VC-targeted PB-to-PVN neurons ( $n = 3$ –4 mice, analyzed at bregma  $-5.1$ – $-4.9$ ).
- (D) Representative images of neurons in the PB (bregma  $-5.1$  mm) that synapse with VC neurons and project to the PVN (VC-targeted PB-to-PVN neurons). White arrows show FoxP2<sup>+</sup> VC-targeted PB-to-PVN neurons that are activated by IL-1 $\beta$  (c-Fos<sup>+</sup>). Scale bar is 200  $\mu$ m.
- (E) Proportion of PB-to-PVN neurons (mCherry<sup>+</sup>, AAVretro-mCherry into the PVN as in Figure S4) expressing Pdyn (green), and conversely, the proportion of Pdyn<sup>+</sup> neurons being PB-to-PVN neurons (red,  $n = 3$  mice).
- (F) Representative images of PB-to-PVN neurons (bregma  $-5.1$  mm) and co-expression of Pdyn. Yellow arrows show Pdyn<sup>+</sup> PB-to-PVN neurons. Scale bar is 200  $\mu$ m.
- (G) Strategy to detect PB-to-PVN presynaptic neurons in the VC. Rabies-EnvA- $\Delta$ G-mCherry viruses infect and replicate only in PB-to-PVN neurons expressing G and TVA proteins («starter neurons»), and retrogradely label presynaptic neurons.
- (H and I) Proportion of «starter neurons» (GFP<sup>+</sup>mCherry<sup>+</sup>) within PB-to-PVN neurons (GFP<sup>+</sup>) or Rabies-infected neurons (mCherry<sup>+</sup>) ( $n = 5$  mice) (H), and a representative image of «starter neurons» (yellow) in the PB (I). Scale bar is 200  $\mu$ m.
- (J and K) Number of PB-to-PVN presynaptic neurons along the rostrocaudal axis of the VC (the obex is at bregma  $-7.2$  mm) (J), and a representative image of presynaptic neurons in the VC (bregma  $-7.44$  mm) indicated by red arrows (K). Scale bar is 200  $\mu$ m.
- (L and M) Selective labeling of VC-to-PB neurons with a DREADD (hM3D(Gq)-mCherry) virus (L), and the CS response induced by intraperitoneal CNO injection (M). Data are mean  $\pm$  SEM. Two-way ANOVA ( $n = 4$ –6 mice per group), ns = not significant, \* $p < 0.05$ , \*\* $p < 0.01$ , and \*\*\* $p < 0.001$  compared with mCherry). See Table S1 for statistics.
- (N) Representative images of VC-to-PB neurons in the VC (left), and mCherry<sup>+</sup> fibers projecting to the PB (right). Scale bar is 200  $\mu$ m.
- (O and P) Selective labeling of VC-targeted PB-to-PVN neurons with a DREADD (hM3D(Gq)-mCherry) virus (O), and the CS response induced by intraperitoneal CNO injection (P). Data are mean  $\pm$  SEM, two-way ANOVA ( $n = 6$ –8 mice per group), ns = not significant, \* $p < 0.05$ , \*\* $p < 0.01$ , and \*\*\* $p < 0.001$  compared with mCherry). See Table S1 for statistics.
- (Q) Representative images of VC-targeted PB-to-PVN neurons and CNO-induced c-Fos in hM3D(Gq)-mCherry or mCherry controls. Scale bar is 200  $\mu$ m.



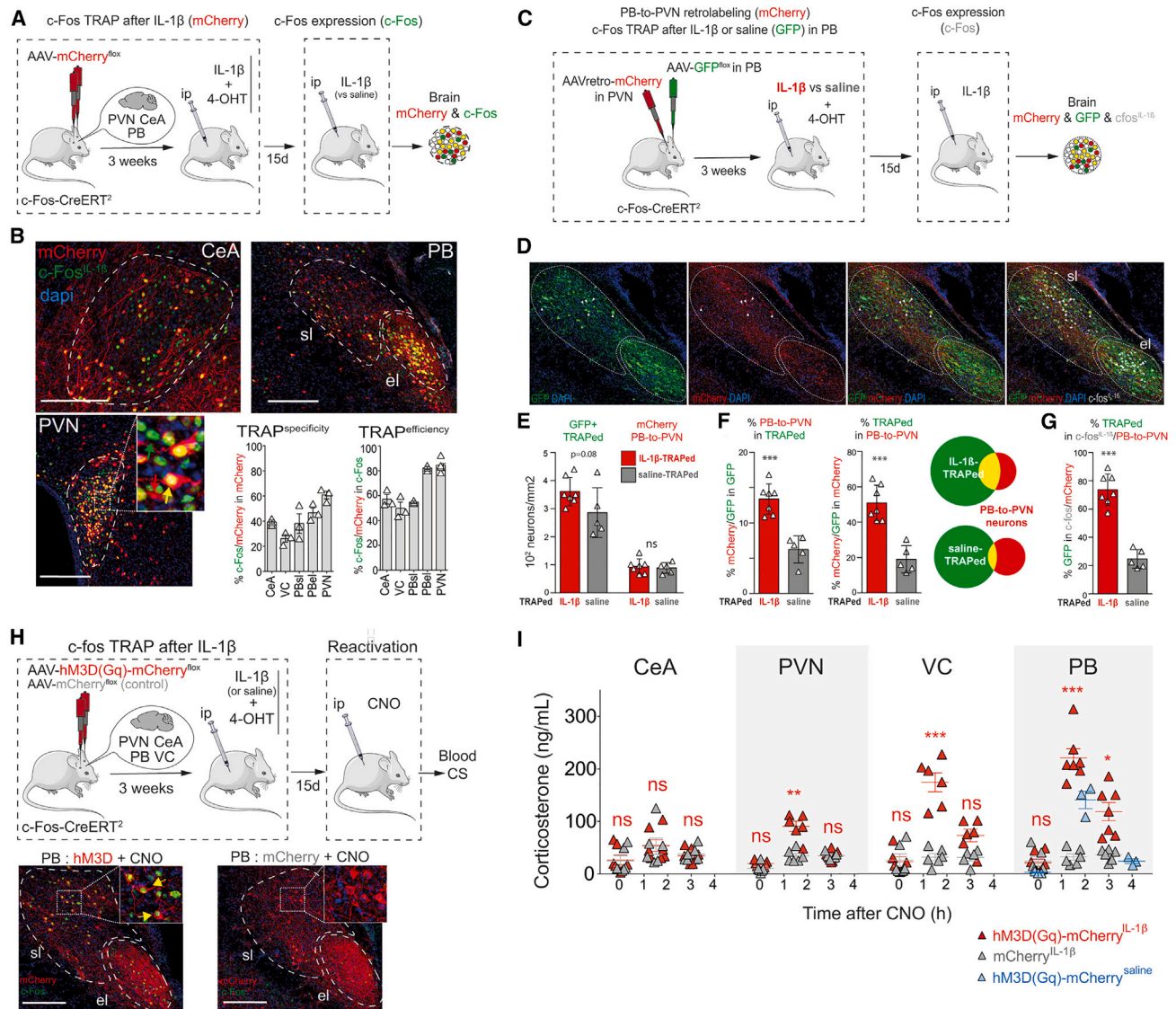


**Figure 6. IL-1 $\beta$ -TRAPed neurons in the PB efficiently induce the corticosterone response**

(A) Procedure for labeling neurons activated by IL-1 $\beta$  (TRAP) in the PVN, CeA, VC, and PB. Transgenic c-Fos-CreERT2 mice are stereotactically injected with a Cre-dependent mCherry AAV. After 3 weeks, neurons are activated by injection of IL-1 $\beta$  and labeled with 4-OHT injection 1h later. After 2 weeks, mice are challenged with IL-1 $\beta$ , and IL-1 $\beta$ -induced c-Fos and TRAPed mCherry<sup>+</sup> neurons are analyzed by immunofluorescence.

(B) Representative images of IL-1 $\beta$ -TRAPed mCherry<sup>+</sup> and IL-1 $\beta$ -activated c-Fos<sup>+</sup> neurons. Arrows show single-positive neurons (green arrow for c-Fos<sup>+</sup>; red arrow for mCherry<sup>+</sup>) and c-Fos<sup>+</sup>mCherry<sup>+</sup> (yellow arrow) neurons. Scale bar is 200  $\mu$ m. Bottom right, ratio of double-positive mCherry<sup>+</sup> c-Fos<sup>+</sup> neurons among mCherry<sup>+</sup> neurons, representing TRAP specificity, and among c-Fos<sup>+</sup> neurons, representing TRAP efficiency (n = 3 mice per group, mean  $\pm$  SEM).

(C and D) Viral strategy to specifically label IL-1 $\beta$ -TRAPed PB neurons, PB-to-PVN neurons, and IL-1 $\beta$ -induced c-Fos<sup>+</sup> neurons (C), with representative pictures of the triple-labeling (D).

(E) Quantification of the density of GFP+ TRAPed neurons (left) and retrogradely labeled PB-to-PVN neurons (right) following TRAPing with IL-1 $\beta$  (red, n = 7) and saline (gray, n = 5) in the PBsl. Data are mean  $\pm$  SEM. See Table S1 for statistics.

(F) Left, quantification of the proportion of double-labeled mCherry+/GFP+ neurons among all GFP+ TRAPed neurons following TRAPing with IL-1 $\beta$  (red, n = 7) and saline (gray, n = 5) in the PBsl. Middle, proportion of double-labeled mCherry+/GFP+ neurons among all mCherry+ PB-to-PVN neurons following TRAPing with IL-1 $\beta$  (red, n = 7) and saline (gray, n = 5) in the PBsl. Data are mean  $\pm$  SEM. Right, representative diagram of the mean relative overlap between PB-to-PVN (red) and TRAPed (green) neuronal populations after TRAPing with IL-1 $\beta$  (top) or saline (bottom). See Table S1 for statistics.

(G) Quantification of the proportion of GFP+/mCherry+ neurons co-expressing IL-1 $\beta$ -induced c-Fos among all mCherry+/c-Fos+ neurons following TRAPing with IL-1 $\beta$  (red, n = 7) or saline (gray, n = 5) in the PBsl. Data are mean  $\pm$  SEM. See Table S1 for statistics.

(H) Top, genetic strategy to pharmacogenetically reactivate IL-1 $\beta$ -TRAPed neurons. Following TRAP, hM3D(Gq)-expressing neurons (or mCherry control neurons) were stimulated by clozapine N-oxide (CNO) injection, and corticosterone (CS) levels were determined. Bottom, representative image of IL-1 $\beta$ -TRAPed PB neurons expressing either hM3D-mCherry (left) or mCherry (right) and treated with CNO. Arrows show CNO-induced c-Fos expression in neurons (yellow). Scale bar: 200  $\mu$ m.

(legend continued on next page)



57.2%  $\pm$  8.7% of all PB-to-PVN neurons (Figures S4A–S4C). FoxP2, a transcription factor abundantly expressed within the PBsl, was expressed by up to 48.5%  $\pm$  6.9% of VC-targeted PB-to-PVN neurons (Figures 5C, 5D, and S4B–S4D). Moreover, IL-1 $\beta$  efficiently induced c-Fos expression in FoxP2-expressing VC-targeted PB-to-PVN neurons (51.9%  $\pm$  11.1%, Figures 5C and 5D). To further characterize PB-to-PVN neurons, we assessed the expression of Pdyn, which labels a subpopulation of FoxP2 neurons involved in nocifensive behaviors.<sup>26,32,33</sup> Pdyn neurons accounted for 30.0%  $\pm$  4.8% of all PB-to-PVN neurons and a large proportion of all Pdyn neurons of the PBsl projected to the PVN (70.0%  $\pm$  6.0%, Figures 5E, 5F, S4E, and S4F).

To characterize the VC neurons synapsing onto PB-to-PVN neurons, we used Cre-dependent monosynaptic rabies trans-synaptic tracing (Figures 5G–5I). From PV-to-PVN starter neurons, we found presynaptic mCherry<sup>+</sup> neurons in the VC, mostly in the NTS, and fewer in the AP (Figures 5J and 5K). VC neurons did not express tyrosine hydroxylase (TH; Figure S4G), thus confirming that PB-to-PVN presynaptic neurons in the NTS were distinct from catecholaminergic VC neurons that project directly to the PVN.<sup>34</sup>

We finally assessed whether the VC-to-PB circuit was sufficient to induce the CS response, using dual stereotaxic injections of retrograde AAVs into the PB and conditional hM3D(Gq)-expressing AAVs into the VC (Figures 5L–5N). We observed a vigorous and prolonged CS response induced by the activation of VC-to-PB neurons only (Figure 5M). The VC-to-PB neurons were found both in the NTS and AP and massively projected to the PBsl as well as to PBel (Figure 5N). To selectively activate the VC-to-PB-to-PVN circuit, we used an intersectional strategy based on both Cre and Flipase-dependent expression to express the hM3D(Gq) receptor in VC-targeted PB-to-PVN neurons (Figure 5O). Upon CNO injection, VC-targeted PB-to-PVN neurons expressed c-Fos and induced the CS response (Figures 5P and 5Q). Finally, we tested whether VC-to-PB and PB-to-PVN neurons were necessary for the IL-1 $\beta$ -induced CS response. The targeted silencing of VC-to-PB or PB-to-PVN neurons with CNO-inducible inhibitory hM4D(Gi) receptor did not significantly alter the IL-1 $\beta$ -induced CS response (Figure S5). Altogether, our data demonstrate that the VC-to-PB-to-PVN circuit is sufficient, but not necessary, to trigger the CS response.

#### Activation modality of the VC-to-PB-to-PVN circuit by IL-1 $\beta$

Most VC neurons that synapse with PB-to-PVN neurons were found in the NTS, the first relay of the vagus nerve in the brain. Thus, we assessed whether the nodose neurons of the vagus nerve activate the VC-to-PB-to-PVN pathway in response to IL-1 $\beta$ . First, we performed a chemical ablation of TRPV1<sup>+</sup> sensory neurons of the dorsal root ganglia (DRG) and nodose ganglia of the vagus using resiniferatoxin (RTX; Figure S6A). RTX administration induced a significant decrease in the number

of TRPV1<sup>+</sup> neurons in the DRG (Figures S6B and S6C), which was sufficient to fully abort heat-induced pain sensation (Figure S6D). RTX also drastically reduced the proportion of TRPV1<sup>+</sup> neurons in the nodose ganglia (Figures S6E and S6F, 25.6%  $\pm$  5.8% of the total neurons to 6.2%  $\pm$  1.4% after RTX), leading to a massive reduction of NTS vagal innervation, as determined by the use of isolectin B4 (IB4), a marker of vagal C-fibers, the predominant fibers of vagus sensory neurons (Figures S6G and S6H).<sup>35</sup> However, such chemical ablation of sensory neurons failed to affect brain activation and the CS response to IL-1 $\beta$  (Figures S6I and S6J), indicating that TRPV1<sup>+</sup> vagal neurons and nociceptors do not play a role in the IL-1 $\beta$ -mediated CS response. To confirm this observation, we performed a bilateral subdiaphragmatic section of the vagus nerve (Figures S6K and S6L). Again, we failed to observe a significant impact on the CS response and the level of c-Fos expressed in the NTS, PBsl, and PVN in response to IL-1 $\beta$ , except at later time points (Figures S6M–S6O). These results indicate that the vagus nerve is not necessary to activate brain neurons and the CS response in response to intraperitoneal injections of IL-1 $\beta$ .

In circumventricular regions of the brain, endothelial cells can respond to IL-1 $\beta$  and relay the activation signal to neurons via the production of the prostaglandin.<sup>36</sup> We thus examined whether the AP, a circumventricular region of the VC in contact with the blood circulation, is activated by IL-1 $\beta$ . Using a GFP-expressing mouse line reporting the activation of the NF- $\kappa$ B pathway, we found IL-1 $\beta$ -induced GFP expression in the AP, as early as 2 h after injection, but not in the NTS or the PB (Figures S6P and S6Q). GFP<sup>+</sup> cells were located close to blood vessels and expressed Cox2, an enzyme required to produce prostaglandins (Figures S6R and S6S). In complement to the neuronal c-Fos mapping, these data show an early activation of non-neuronal Cox2<sup>+</sup> cells in AP in response to IL-1 $\beta$ .

#### The reactivation of PB neurons activated by IL-1 $\beta$ induces the CS response

We next tested whether PB neurons activated by IL-1 $\beta$  can induce the CS response when specifically reactivated. To this end, we used the c-Fos-CreERT2 mouse line for targeted activity-dependent expression of a reporter protein in IL-1 $\beta$ -activated neurons. In this transgenic line, neuronal activation results in the expression of CreER, which enters the nucleus when bound to 4-hydroxytamoxifen (4-OHT), the administration of which temporally gates the window of recombination and permanent labeling (or “TRAPing”) of activated neurons.<sup>37</sup> In preliminary experiments, we determined that administration of 4-OHT 1 h after IL-1 $\beta$  injection was the optimal time setting to capture IL-1 $\beta$ -activated neurons (Figures S7A–S7C). We then performed genetic labeling of IL-1 $\beta$ -activated neurons (“IL-1 $\beta$ -TRAPed neurons”) in the PB as well as in the regions most recruited by IL-1 $\beta$  and connected to the PB, such as PVN, CeA, and VC. First, to assess the efficiency and specificity of IL-1 $\beta$ -mediated labeling, IL-1 $\beta$

(I) CS blood levels following CNO-induced reactivation of IL-1 $\beta$ -TRAPed CeA, PVN, VC, and PB neurons (red, hM3D-mCherry; gray, control mCherry) and saline-TRAPed PB neurons (blue). All groups were treated with CNO. Data are mean  $\pm$  SEM. Two-way ANOVA ( $n = 6$ – $7$  mice per group for the 3 respective brain regions), ns = not significant, \* $p < 0.05$ , \*\* $p < 0.01$ , and \*\*\* $p < 0.001$  compared with mCherry<sup>IL-1 $\beta$</sup>  (see Table S1 for statistics). The saline-TRAPed data are also represented in Figure S7I (see Table S1 for statistics).

was reinjected 2 weeks after initial genetic labeling of neurons with IL-1 $\beta$  (Figures 6A and B), and the neurons expressing both the reporter (mCherry) and the protein c-Fos were quantified. As a measure of genetic labeling efficiency, 40%–60% of c-Fos<sup>+</sup> neurons in CeA, PB, VC, and PVN also expressed the mCherry reporter (Figure 6B). As a measure of genetic labeling specificity, 50%–80% of genetically labeled neurons re-expressed the protein c-Fos (Figure 6B), similar to the previously reported data.<sup>37</sup>

We investigated the identity of IL-1 $\beta$ -TRAPed PB neurons and whether they included PB-to-PVN neurons. Following IL-1 $\beta$ -TRAPing, we observed labeled neurons in both the PBsl and PBel and detected axonal projections to the PVN, the BST, and CeA (Figures S7D and S7E). We thus combined AAV retrograde tracing with the TRAP system to label PB-to-PVN neurons and IL-1 $\beta$ -TRAPed PB neurons, respectively (Figures 6C–6E). Although less than 15% of IL-1 $\beta$ -TRAPed PB neurons were PB-to-PVN neurons, we found that half (50.9%  $\pm$  3.7%) of the PB-to-PVN neurons were TRAPed by IL-1 $\beta$ , whereas only a limited proportion PB-to-PVN neurons (18.9%  $\pm$  3.4%) were TRAPed by saline (Figures 6F, S7G, and S7H) and mineral oil used for the administration of 4-OHT (Figures S7I and S7J). As an additional measure of TRAPing specificity, we reinjected IL-1 $\beta$  to induce the expression of the c-Fos and observed that the large majority of PB-to-PVN neurons expressing c-Fos were previously TRAPed with IL-1 $\beta$  (73.7%  $\pm$  4.2%), whereas saline/vehicle-TRAPed neurons showed limited overlap with c-Fos<sup>+</sup> PB-to-PVN neurons (24.7%  $\pm$  2.9%; Figure 6G). We thus concluded that IL-1 $\beta$ -TRAPed PB neurons efficiently engaged the PB-to-PVN circuit, whereas control saline/vehicle-TRAPed PB neurons did not.

We then used this TRAP approach to assess whether PB neurons activated by IL-1 $\beta$  can induce the CS response. TRAPed PB neurons, as well as TRAPed VC, CeA, or PVN neurons, were selectively transduced to express the G-protein-coupled hMD3D(Gq) receptor (Figure 6H). The reactivation by CNO of IL-1 $\beta$ -TRAPed neurons in the PB promptly induced a vigorous and prolonged CS response (Figure 6I). Significant levels of CS were also induced by the reactivation of IL-1 $\beta$ -TRAPed neurons in the VC (upstream of PB) or PVN (downstream of PB), but not in CeA (Figures 6H and 6I). Reactivation of saline/vehicle-TRAPed PB neurons induced a significant but short-lived CS response (Figures 6I and S7K). Finally, in accordance with our previous observation (Figure S5), we found that IL-1 $\beta$ -TRAPed PB neurons were sufficient but not necessary to induce a CS response, as the targeted ablation of IL-1 $\beta$ -TRAPed PB neurons with the apoptosis-inducing Caspase 3 did not significantly alter the IL-1 $\beta$ -induced CS response (Figures S7L–S7N). Altogether, these results demonstrate that IL-1 $\beta$  recruits a specific VC-to-PB-to-PVN neuronal circuit that induces the CS response when reactivated.

### Activation of the PB-to-PVN circuit mediates the suppression of immune cell development

CS is the quintessential immunosuppressive hormone, regulating the development of immune cells and the level of inflammatory responses. However, multiple checkpoints control the systemic activity of CS.<sup>6</sup> To assess whether the CS response

evoked by IL-1 $\beta$ -activated PB neurons is sufficient to modulate immunity, we assessed the impact of PB circuit activation on three well-described CS-sensitive developmental processes, the maturation of T cell precursors in the thymus,<sup>38</sup> the maturation of B cell precursors in the bone marrow,<sup>39</sup> and the release of granulocytes into the blood.<sup>40</sup>

To this end, we activated IL-1 $\beta$ -TRAPed PB neurons for 2 days using DREADD stimulation of hMD3(Gq)-expressing neurons and analyzed immune cells by flow cytometry (Figures 7A and S8). DREADD-activated IL-1 $\beta$ -TRAPed PB neurons were compared with mCherry-expressing IL-1 $\beta$ -TRAPed PB neurons exposed to identical CNO treatment. As an additional control, we assessed the activation of DREADD-expressing IL-1 $\beta$ -TRAPed neurons in CeA, a region strongly activated by IL-1 $\beta$  and involved in the behavioral response to stress, pain, and inflammation but not in CS response. Following CNO administration, we observed significant thymus shrinking (Figure 7B), due mostly to decreased numbers of immature CD4<sup>+</sup>CD8<sup>+</sup> T cells. Bone marrow B cell precursors, in particular resting pre-B and transitional B cells, were similarly reduced (Figures 7D and 7J), leading to a decrease in circulating B cells. Finally, the frequencies of eosinophils and basophils were significantly decreased in the blood,<sup>41</sup> whereas neutrophil numbers were slightly increased (Figures 7F, 7H, and 7I). By contrast, reactivation of IL-1 $\beta$ -TRAPed neurons in the CeA did not affect the generation of thymocytes, B cells, and granulocytes (Figures 7C, 7E, and 7G), in accordance with the absence of CS response after the reactivation of IL-1 $\beta$ -TRAPed CeA neurons (Figures 6I and 6J). Taken together, these results show that the CS response evoked by IL-1 $\beta$ -activated PB neurons is sufficient to induce CS-mediated systemic immunosuppression.

## DISCUSSION

We show here that the type-3 pro-inflammatory cytokines IL-1 $\beta$  and TNF- $\alpha$ —but not type-1 or type 2 cytokines—induce c-Fos activation in specific brain circuits leading to CS release. We dissected the circuit engaged in the coupling of IL-1 $\beta$  sensing with the CS response and identified a subpopulation of PB neurons that receives inputs from the VC and projects to the PVN. These PB-to-PVN neurons, a majority of which express FoxP2 and Pdyn, are responsive to IL-1 $\beta$  but not to nociceptive signals. Our data also indicate that IL-1 $\beta$  sensing in the VC does not rely on sensory vagal inputs or nociceptors. Finally, we demonstrate that the reactivation of PB neurons is sufficient to induce a vigorous CS response and, as a consequence, regulate the development of immune cells in the bone marrow and the thymus.

The PB integrates multiple sensory information from the periphery via the vagus nerve and the spinoparabrachial pathway and coordinates diverse autonomic functions, such as fever, glycemia, pleasure, and arousal, as well as behaviors associated with perceived danger.<sup>12,14,15,25,33</sup> We show that the PB also integrates information on blood levels of pro-inflammatory cytokines to induce the CS response. Given the diversity of sensory inputs reaching the PB, the PB must integrate multiple pathways, acting synergistically or in opposition, to trigger the CS response. Here, we did not detect a significant impact of

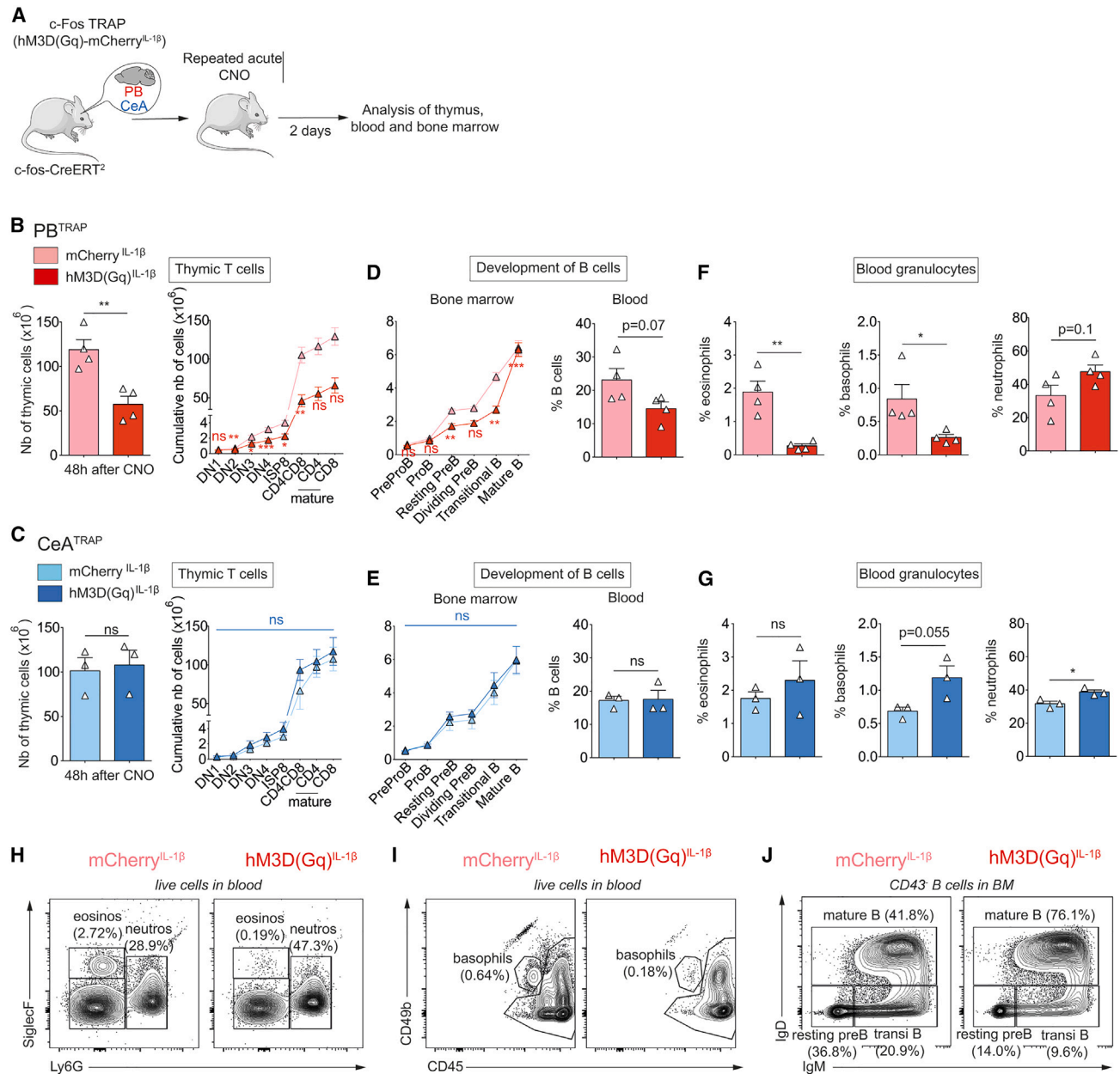


**Figure 7. Activation of IL-1 $\beta$ -TRAPed neurons in the PB induces systemic immunosuppression**

(A) Procedure for labeling neurons activated by IL-1 $\beta$  in the PB (PB<sup>TRAP</sup>, n = 4 mice per group) or CeA (CeA<sup>TRAP</sup>, n = 3 mice per group), and restimulation of the neurons for 2 days with CNO. Thymic, blood, and bone marrow (BM) cells were harvested, processed, and analyzed by flow cytometry.

(B and C) Total thymocyte numbers (left) and cumulative numbers of immature to mature thymocytes (right) in PB<sup>TRAP</sup> (B) or CeA<sup>TRAP</sup> (C) mice. DN: CD4<sup>+</sup>CD8<sup>+</sup> double negative cells. ISP8: immature single-positive CD8 T cells. t test for number of thymic cells and cumulative number of subpopulations, ns = not significant, \*p < 0.05, \*\*p < 0.01 and \*\*\*p < 0.001 compared with mCherry<sup>IL-1β</sup> group. Data are mean  $\pm$  SEM.

(D and E) Cumulative numbers of immature and mature B cells in the bone marrow (left), and frequency of B cells in the blood (right) of PB<sup>TRAP</sup> (D) or CeA<sup>TRAP</sup> (E) mice. t test for number of blood B cells and the cumulative number of thymic cells, ns = not significant, \*p < 0.05, \*\*p < 0.01, and \*\*\*p < 0.001 compared with mCherry<sup>IL-1β</sup> group. Data are mean  $\pm$  SEM.

(F and G) Frequency of eosinophils, basophils, and neutrophils in the blood of PB<sup>TRAP</sup> (F) or CeA<sup>TRAP</sup> (G) mice. t test, ns = not significant, \*p < 0.05, \*\*p < 0.01, and \*\*\*p < 0.001 compared with mCherry<sup>IL-1β</sup> group. Data are mean  $\pm$  SEM.

(H–J) Representative flow cytometry plots of immune cell populations in IL-1 $\beta$ -TRAPed expressing hM3D(Gq) or mCherry controls.



the vagal and spinoparabrachial pathways on the PB-mediated CS response. Recent work has begun to unravel the input-output diagram of the PB subcircuits, illustrating how PB subpopulations are wired from specific routed sensory inputs to specific brain outputs. For instance,  $\text{SatB2}^+$  PB neurons were shown to relay gustatory inputs to the gustatory thalamus,<sup>42</sup> whereas  $\text{CGRP}^+$ ,  $\text{Tac1}^+$ ,  $\text{Pdyn}^+$ , and  $\text{FoxP2}^+$  PB neurons integrate nociceptive, noxious, and feeding inputs to induce aversive and nocifensive responses.<sup>14,20,25,32</sup> Half of the  $\text{Pdyn}^+$  neuronal population also includes heat-activated neurons involved in heat defense behaviors.<sup>33</sup> In this study, we found that a subpopulation of the PB integrates inflammatory signals to control the CS response via the PVN. This dedicated PB-to-PVN circuit expresses  $\text{FoxP2}$  and  $\text{Pdyn}$ , but not  $\text{CGRP}$ . These neurons fail to respond to prolonged noxious TRPV1-dependent signals from the spinoparabrachial pathway (Figure S3) but are activated by acute foot shock (Figure S2E). These data suggest the existence of a functional subdivision within the  $\text{Pdyn}$  population, one driving the CS response to inflammatory signals and another driving escape behaviors in response to noxious stimuli. Dissecting the  $\text{Pdyn}/\text{FoxP2}$  neuronal population in the PB will be critical to define their receptive field and functions in the regulation of neuroendocrine/sympathetic outputs.

It has been shown previously that catecholaminergic neurons of the medulla are necessary for the CS response to IL-1 $\beta$  and LPS.<sup>19,43,44</sup> TH-expressing neurons are found both in the RVM and the NTS<sup>34,43,45</sup> and project directly to the PVN and to  $\text{CGRP}^+$  neurons in the PBel.<sup>46</sup> Although we showed that TH<sup>+</sup> NTS cells are poorly recruited by IL-1 $\beta$  (Figure S1C and S1D), our study does not address the relative impact of the direct catecholaminergic NTS/RVM-to-PVN pathway compared with the NTS-to-PB-to-PVN pathway. Furthermore, we find that the VC-to-PB-to-PVN pathway is sufficient but not necessary to induce the CS response (Figures S5 and S7L–S7N). The absence of effects of such loss-of-function manipulations may suggest the co-existence of alternative and redundant pathways to trigger the CS response but does not rule out specific contexts in which these different pathways are necessary. This also suggests that the VC conveys multiple chemical and physical stress signals (inflammatory, pain, cardio-vascular, and metabolic) that may interact to activate diverse pathways.<sup>47</sup> Future experiments will determine in which contexts the NTS catecholaminergic and PB pathways are, respectively, engaged to activate the CS response, their relative contribution in the amplitude and kinetics of the CS response, as well as their possible mutual regulation in neuronal output to the PVN. As the PB is necessary for associative taste memory<sup>20</sup> and receives direct inputs from the insular cortex, a region known to regulate the immune system based on previous experiences,<sup>5</sup> it may be proposed that the PB-to-PVN circuit is engaged during the recall of memory associated with previous inflammatory events.

We found that the TRAPing of PB neurons following IL-1 $\beta$  injection led to an effective recruitment of the PB-to-PVN circuit, prolonged release of CS, and peripheral immunosuppression. In that experiment, CNO-induced reactivation of DREADD-expressing IL-1 $\beta$ -TRAPed PB neurons was compared with mCherry-expressing IL-1 $\beta$ -TRAPed neurons, in order to control for the potential immunomodulatory effect of CNO. Reactivation

of IL-1 $\beta$ -TRAPed neurons in the PB was also compared with the reactivation of IL-1 $\beta$ -TRAPed neurons in the CeA, the latter being involved in the behavioral response to stress, pain, and inflammation, including IL-1 $\beta$ , but not involved in the CS response. A third type of control may have quantified the effect of reactivation of saline-TRAPed PB neurons. Indeed, saline-TRAPed neurons were abundant in the PB (Figures S7G and S7H), as were neurons activated by the vehicle used for TRAPing (Figures S7I and S7J). However, although DREADD-activation of saline-TRAPed PB neurons led to a transient but short-lived CS response (Figures 6I and S7K), saline did not significantly recruit the PB-to-PVN circuit (Figures 6F and S7I). It is therefore possible that saline/vehicle injections induce a PB-dependent CS response via neuronal circuits other than the PB-to-PVN circuit, probably involving activators distinct from cytokines. Together with the absence of effects of the loss-of-function experiments, these elements confirm the co-existence of alternative and redundant pathways to trigger the CS response.

Previous studies have shown that the NTS is a critical brain portal for inflammatory signals to induce the CS response.<sup>48</sup> As vagus afferents to the NTS are involved in cytokine-induced fever<sup>49</sup> (see also ref.<sup>3</sup>), it has been suggested that the vagus nerve is similarly involved in the cytokine-induced CS response. However, it has also been proposed that for high levels of cytokines circulating in the blood and cerebrospinal fluid, the detection may occur in circumventricular and perivascular organs, such as the AP.<sup>45</sup> In that context, perivascular cells expressing cytokine receptors respond to cytokines by the activation of the NF- $\kappa$ B pathway and the production of prostaglandins.<sup>50</sup> In accordance with this view, activation of PVN neurons<sup>51,52</sup> and the CS response<sup>53,54</sup> by high doses of IL-1 $\beta$  or LPS injected into the peritoneum is affected by the inhibition of prostaglandin production and is associated with increased expression of *Cox2* and NF- $\kappa$ B transcripts in the AP.<sup>51,55</sup> In the present manuscript, we also observed that IL-1 $\beta$  directly or indirectly activates the NF- $\kappa$ B pathway in perivascular cells of the AP and that *Cox2* is highly expressed in the AP. A local loss-of-function approach would complement our study in order to determine whether the AP directly senses IL-1 $\beta$  and contributes to the IL-1 $\beta$ -induced CS response.<sup>56,57</sup>

We show that the PB-centered pathway inducing the CS response is efficiently triggered by IL-1 $\beta$  and TNF $\alpha$ , as well as by the bacterial compound LPS that induces the production of these anti-microbial cytokines. By contrast, the CS response is poorly induced by cytokines produced in response to viral and intracellular infections, such as IL-12 and IFN $\gamma$ , or in response to cytokines produced in response to helminths or allergens, such as IL-33, IL-4, and IL-13. Of note, the vagus sensory neurons express cytokine receptors and amplify, for example, pro-allergic responses in the lung through the local release of neuropeptides.<sup>58</sup> However, it is not known whether, in addition to this local neuro-immune reflex, information related to lung allergy is transmitted by the vagus to the NTS and subsequent brain circuits. Furthermore, type I interferons IFN $\alpha$  and IFN $\beta$ , produced early in the response to cellular infections, induce fever, however, at a relatively low level compared with IL-1 $\beta$ .<sup>59</sup> We speculate that anti-microbial responses are efficiently sensed by the brain because they reflect a systemic danger to the individual to which

the brain has to respond by concerted actions including fever, sickness behavior, and CS response. As an example of the lethality of uncontrolled anti-microbial immune responses, a septic shock mediated by LPS and the induction of IL-1 $\beta$  and TNF $\alpha$  rapidly leads to multi-organ failure if not controlled by prompt anti-inflammatory measures.<sup>60</sup> IL-1 $\beta$  is processed from pro-IL-1 $\beta$  by the inflammasome, which is activated in the cytoplasm by the loss of cellular integrity.<sup>61</sup> The released IL-1 $\beta$  is further amplified by IL-1 $\beta$ -induced IL-1 $\beta$ -release that increases the circulating levels of IL-1 $\beta$ .<sup>62</sup> It is therefore possible that cell death and the dissemination of microbes pose a considerable danger to the organism to which the organism best responds by a systemic effort coordinated by the brain to orchestrate immune, metabolic, and behavioral responses, in contrast to more local viral and parasitic infections.

In conclusion, we have discovered a dedicated pathway by which pro-inflammatory and anti-microbial cytokines induce the CS response via the PB. As the PB is a key hub for interoceptive and exteroceptive sensory inputs to diverse autonomic outputs and behavioral centers, it is tempting to speculate that the PB integrates various pro-inflammatory and sensory experiences to optimize the amplitude and duration of the CS response. Thus, new approaches to regulate peripheral inflammation may be proposed that target the activity of the PB via the VC to ultimately regulate the CS response.

## STAR★METHODS

Detailed methods are provided in the online version of this paper and include the following:

- KEY RESOURCES TABLE
- RESOURCE AVAILABILITY
  - Lead contact
  - Materials availability
  - Data and code availability
- EXPERIMENTAL MODEL AND SUBJECT DETAILS
- METHOD DETAILS
  - Cytokine and neuromodulator preparation
  - Drug preparation
  - Tail-flick antinociception test
  - Blood sampling and corticosterone measurements
  - Subdiaphragmatic vagotomy
  - Stereotaxic injections of viral vectors
  - In vivo calcium recording with fiber photometry
  - Histology and immunostaining
  - Image processing and analysis
  - Flow cytometry
- QUANTIFICATION AND STATISTICAL ANALYSIS

## SUPPLEMENTAL INFORMATION

Supplemental information can be found online at <https://doi.org/10.1016/j.neuron.2023.05.009>.

## ACKNOWLEDGMENTS

We would like to thank Robert Dantzer (MD Anderson Center) for advice and mentorship, Françoise Guinet (Institut Pasteur) for support on flow cytometry,

Lucie Peduto (Institut Pasteur) and Adam Benabid (Institut Pasteur) for Apo-tome microscopy, Gré and GENIE project and the Janelia Farm Research Campus for sharing GCamp constructs.

This work was funded by the French Ministry of Higher Education and Research. Lledo's lab is supported by the Life Insurance Company AG2R-La Mondiale and MTRL. Eberl's lab is supported by Inserm and Institut Pasteur. Eberl's and Lledo's labs are supported by Agence National de la Recherche (ANR-21-CE15-0003 "Brainity"). Conzelmann's lab is supported by the German Research Foundation (DFG)—Project-ID 369799452TRR237 A12 and Project-ID 118803580—SFB 870 Z1. A.J.C. was supported by the PPU program of the Institut Pasteur.

## AUTHOR CONTRIBUTIONS

F.J., G.L., P.-M.L., and G.E. conceived the projects and designed the experiments. F.J. conceived and performed most of the experiments. G.L. performed calcium-recording experiments. M.P. and F.J. performed vagus nerve studies. R.G.-B., A.J.C., L.B., G.L., and R.D.-D. performed histological and blood sampling experiments. K.-K.C. provided the Rabies virus and helped with the virus tracing experiments. F.J. analyzed the data. F.J., G.E., and G.L. wrote the paper.

## DECLARATION OF INTERESTS

The authors declare no competing interests.

## INCLUSION AND DIVERSITY

We support inclusive, diverse, and equitable conduct of research.

Received: March 22, 2021

Revised: April 13, 2023

Accepted: May 10, 2023

Published: June 5, 2023

## REFERENCES

1. Metalnikov, S., and Chorine, V. (1926). Rôle des réflexes conditionnels dans l'immunité. *Ann. Inst. Pasteur CLXXXII*, 1640.
2. Dantzer, R. (2018). Neuroimmune interactions: from the brain to the immune system and vice versa. *Physiol. Rev.* 98, 477–504. <https://doi.org/10.1152/physrev.00039.2016>.
3. Ilanges, A., Shiao, R., Shaked, J., Luo, J.-D., Yu, X., and Friedman, J.M. (2022). Brainstem ADCYAP1<sup>+</sup> neurons control multiple aspects of sickness behaviour. *Nature* 609, 761–771. <https://doi.org/10.1038/s41586-022-05161-7>.
4. Osterhout, J.A., Kapoor, V., Eichhorn, S.W., Vaughn, E., Moore, J.D., Liu, D., Lee, D., DeNardo, L.A., Luo, L., Zhuang, X., and Dulac, C. (2022). A pre-optic neuronal population controls fever and appetite during sickness. *Nature* 606, 937–944. <https://doi.org/10.1038/s41586-022-04793-z>.
5. Koren, T., Yifa, R., Amer, M., Krot, M., Boshnak, N., Ben-Shaanan, T.L., Azulay-Debby, H., Zalayat, I., Avishai, E., Hajjo, H., et al. (2021). Insular cortex neurons encode and retrieve specific immune responses. *Cell* 184, 6211. <https://doi.org/10.1016/j.cell.2021.11.021>.
6. Cain, D.W., and Cidlowski, J.A. (2017). Immune regulation by glucocorticoids. *Nat. Rev. Immunol.* 17, 233–247. <https://doi.org/10.1038/nri.2017.1>.
7. Beurel, E., and Nemeroff, C.B. (2014). Interaction of stress, corticotropin-releasing factor, arginine vasopressin and behaviour. *Curr. Top. Behav. Neurosci.* 18, 67–80. [https://doi.org/10.1007/7854\\_2014\\_306](https://doi.org/10.1007/7854_2014_306).
8. Ziegler, D.R., and Herman, J.P. (2002). Neurocircuitry of stress integration: anatomical pathways regulating the hypothalamo-pituitary-adrenocortical axis of the rat. *Integr. Comp. Biol.* 42, 541–551. <https://doi.org/10.1093/icb/42.3.541>.

9. Turnbull, A.V., and Rivier, C.L. (1999). Regulation of the hypothalamic-pituitary-adrenal axis by cytokines: actions and mechanisms of action. *Physiol. Rev.* 79, 1–71. <https://doi.org/10.1152/physrev.1999.79.1.1>.
10. Larsen, P.J., and Mikkelsen, J.D. (1995). Functional identification of central afferent projections conveying information of acute "stress" to the hypothalamic paraventricular nucleus. *J. Neurosci.* 15, 2609–2627. <https://doi.org/10.1523/JNEUROSCI.15-04-02609.1995>.
11. Silverman, A.J., Hoffman, D.L., and Zimmerman, E.A. (1981). The descending afferent connections of the paraventricular nucleus of the hypothalamus (PVN). *Brain Res. Bull.* 6, 47–61. [https://doi.org/10.1016/s0361-9230\(81\)80068-8](https://doi.org/10.1016/s0361-9230(81)80068-8).
12. Chiang, M.C., Bowen, A., Schier, L.A., Tupone, D., Uddin, O., and Heinricher, M.M. (2019). Parabrachial complex: a hub for pain and aversion. *J. Neurosci.* 39, 8225–8230. <https://doi.org/10.1523/JNEUROSCI.1162-19.2019>.
13. Roman, C.W., Derkach, V.A., and Palmiter, R.D. (2016). Genetically and functionally defined NTS to PBN brain circuits mediating anorexia. *Nat. Commun.* 7, 11905. <https://doi.org/10.1038/ncomms11905>.
14. Barik, A., Thompson, J.H., Seltzer, M., Ghitani, N., and Chesler, A.T. (2018). A brainstem-spinal circuit controlling nociceptive behavior. *Neuron* 100, 1491–1503.e3. <https://doi.org/10.1016/j.neuron.2018.10.037>.
15. Deng, J., Zhou, H., Lin, J.-K., Shen, Z.-X., Chen, W.-Z., Wang, L.-H., Li, Q., Mu, D., Wei, Y.-C., Xu, X.-H., and Sun, Y.-G. (2020). The parabrachial nucleus directly channels spinal nociceptive signals to the intralaminar thalamic nuclei, but not the amygdala. *Neuron* 107, 909–923.e6. <https://doi.org/10.1016/j.neuron.2020.06.017>.
16. Kawashima, T., Okuno, H., and Bito, H. (2014). A new era for functional labeling of neurons: activity-dependent promoters have come of age. *Front. Neural Circuits* 8, 37. <https://doi.org/10.3389/fncir.2014.00037>.
17. Konsman, v., Parnet, P., and Dantzer, R. (2002). Cytokine-induced sickness behaviour: mechanisms and implications. *Trends Neurosci.* 25, 154–159. [https://doi.org/10.1016/s0166-2236\(00\)02088-9](https://doi.org/10.1016/s0166-2236(00)02088-9).
18. Schwarz, L.A., and Luo, L. (2015). Organization of the locus coeruleus-norepinephrine system. *Curr. Biol.* 25, R1051–R1056. <https://doi.org/10.1016/j.cub.2015.09.039>.
19. Weidenfeld, J., Abramsky, O., and Ovadia, H. (1989). Evidence for the involvement of the central adrenergic system in interleukin 1-induced adrenocortical response. *Neuropharmacology* 28, 1411–1414. [https://doi.org/10.1016/0028-3908\(89\)90018-x](https://doi.org/10.1016/0028-3908(89)90018-x).
20. Palmiter, R.D. (2018). The parabrachial nucleus: CGRP neurons function as a general alarm. *Trends Neurosci.* 41, 280–293. <https://doi.org/10.1016/j.tins.2018.03.007>.
21. Ye, J., and Veinante, P. (2019). Cell-type specific parallel circuits in the bed nucleus of the stria terminalis and the central nucleus of the amygdala of the mouse. *Brain Struct. Funct.* 224, 1067–1095. <https://doi.org/10.1007/s00429-018-01825-1>.
22. Wang, Y., Kim, J., Schmit, M., Cho, T., Fang, C., and Cai, H. (2018). A BNST-centered microcircuit regulating inflammation-associated anorexia and feeding. [https://papers.ssrn.com/sol3/papers.cfm?abstract\\_id=3236485](https://papers.ssrn.com/sol3/papers.cfm?abstract_id=3236485).
23. Aoki, M., Shimozuru, M., Kikusui, T., Takeuchi, Y., and Mori, Y. (2010). Sex differences in behavioral and corticosterone responses to mild stressors in ICR mice are altered by ovariectomy in peripubertal period. *Zoolog. Sci.* 27, 783–789. <https://doi.org/10.2108/zsj.27.783>.
24. Schmidt, E.D., Janszen, A.W., Wouterlood, F.G., and Tilders, F.J. (1995). Interleukin-1-induced long-lasting changes in hypothalamic corticotropin-releasing hormone (CRH)-neurons and hyperresponsiveness of the hypothalamus-pituitary-adrenal axis. *J. Neurosci.* 15, 7417–7426. <https://doi.org/10.1523/JNEUROSCI.15-11-07417.1995>.
25. Campos, C.A., Bowen, A.J., Roman, C.W., and Palmiter, R.D. (2018). Encoding of danger by parabrachial CGRP neurons. *Nature* 555, 617–622. <https://doi.org/10.1038/nature25511>.
26. Huang, D., Grady, F.S., Peltekian, L., and Geerling, J.C. (2021). Efferent projections of Vglut2, Foxp2, and Pdyn parabrachial neurons in mice. *J. Comp. Neurol.* 529, 657–693. <https://doi.org/10.1002/cne.24975>.
27. Gunaydin, L.A., Grosenick, L., Finkelstein, J.C., Kauvar, I.V., Fenno, L.E., Adhikari, A., Lammel, S., Mirzabekov, J.J., Airan, R.D., Zalocusky, K.A., et al. (2014). Natural neural projection dynamics underlying social behavior. *Cell* 157, 1535–1551. <https://doi.org/10.1016/j.cell.2014.05.017>.
28. Li, P., Geng, X., Jiang, H., Caccavano, A., Vicini, S., and Wu, J.Y. (2019). Measuring sharp waves and oscillatory population activity with the genetically encoded calcium indicator GCaMP6f. *Front. Cell. Neurosci.* 13, 274. <https://doi.org/10.3389/fncel.2019.00274>.
29. Legaria, A.A., Matikainen-Ankney, B.A., Yang, B., Ahanonu, B., Licholai, J.A., Parker, J.G., and Kravitz, A.V. (2022). Fiber photometry in striatum reflects primarily nonsomatic changes in calcium. *Nat. Neurosci.* 25, 1124–1128. <https://doi.org/10.1038/s41593-022-01152-z>.
30. Sinniger, V., Porcher, C., Mouchet, P., Juhem, A., and Bonaz, B. (2004). c-fos and CRF receptor gene transcription in the brain of acetic acid-induced somato-visceral pain in rats. *Pain* 110, 738–750. <https://doi.org/10.1016/j.pain.2004.05.014>.
31. Zingg, B., Chou, X.-L., Zhang, Z.-G., Mesik, L., Liang, F., Tao, H.W., and Zhang, L.I. (2017). AAV-mediated anterograde transsynaptic tagging: mapping corticocollicular input-defined neural pathways for defense behaviors. *Neuron* 93, 33–47. <https://doi.org/10.1016/j.neuron.2016.11.045>.
32. Chiang, M.C., Nguyen, E.K., Canto-Bustos, M., Papale, A.E., Oswald, A.M., and Ross, S.E. (2020). Divergent neural pathways emanating from the lateral parabrachial nucleus mediate distinct components of the pain response. *Neuron* 106, 927–939.e5. <https://doi.org/10.1016/j.neuron.2020.03.014>.
33. Geerling, J.C., Kim, M., Mahoney, C.E., Abbott, S.B., Agostinelli, L.J., Garfield, A.S., Krashes, M.J., Lowell, B.B., and Scammell, T.E. (2016). Genetic identity of thermosensory relay neurons in the lateral parabrachial nucleus. *Am. J. Physiol. Regul. Integr. Comp. Physiol.* 310, R41–R54. <https://doi.org/10.1152/ajpregu.00094.2015>.
34. Hollis, J.H., Lightman, S.L., and Lowry, C.A. (2005). Lipopolysaccharide has selective actions on sub-populations of catecholaminergic neurons involved in activation of the hypothalamic-pituitary-adrenal axis and inhibition of prolactin secretion. *J. Endocrinol.* 184, 393–406. <https://doi.org/10.1677/joe.1.05839>.
35. Hermes, S.M., Andresen, M.C., and Aicher, S.A. (2016). Localization of TRPV1 and P2X3 in unmyelinated and myelinated vagal afferents in the rat. *J. Chem. Neuroanat.* 72, 1–7. <https://doi.org/10.1016/j.jchemneu.2015.12.003>.
36. Blatteis, C.M., and Li, S. (2000). Pyrogenic signaling via vagal afferents: what stimulates their receptors? *Auton. Neurosci.* 85, 66–71. [https://doi.org/10.1016/S1566-0702\(00\)00221-6](https://doi.org/10.1016/S1566-0702(00)00221-6).
37. Allen, W.E., DeNardo, L.A., Chen, M.Z., Liu, C.D., Loh, K.M., Fenno, L.E., Ramakrishnan, C., Deisseroth, K., and Luo, L. (2017). Thirst-associated preoptic neurons encode an aversive motivational drive. *Science* 357, 1149–1155. <https://doi.org/10.1126/science.aan6747>.
38. Tarcic, N., Ovadia, H., Weiss, D.W., and Weidenfeld, J. (1998). Restraint stress-induced thymic involution and cell apoptosis are dependent on endogenous glucocorticoids. *J. Neuroimmunol.* 82, 40–46. [https://doi.org/10.1016/S0165-5728\(97\)00186-0](https://doi.org/10.1016/S0165-5728(97)00186-0).
39. Laakko, T., and Fraker, P. (2002). Rapid changes in the lymphopoietic and granulopoietic compartments of the marrow caused by stress levels of corticosterone. *Immunology* 105, 111–119. <https://doi.org/10.1046/j.1365-2567.2002.01346.x>.
40. Trottier, M.D., Newsted, M.M., King, L.E., and Fraker, P.J. (2008). Natural glucocorticoids induce expansion of all developmental stages of murine bone marrow granulocytes without inhibiting function. *Proc. Natl. Acad. Sci. USA* 105, 2028–2033. <https://doi.org/10.1073/pnas.0712003105>.
41. Dunskey, E.H., Zweiman, B., Fischler, E., and Levy, D.A. (1979). Early effects of corticosteroids on basophils, leukocyte histamine, and tissue



- histamine. *J. Allergy Clin. Immunol.* 63, 426–432. [https://doi.org/10.1016/0091-6749\(79\)90217-3](https://doi.org/10.1016/0091-6749(79)90217-3).
42. Jarvie, B.C., Chen, J.Y., King, H.O., and Palmiter, R.D. (2021). Satb2 neurons in the parabrachial nucleus mediate taste perception. *Nat. Commun.* 12, 224. <https://doi.org/10.1038/s41467-020-20100-8>.
  43. Bienkowski, M.S., and Rinaman, L. (2008). Noradrenergic inputs to the paraventricular hypothalamus contribute to hypothalamic-pituitary-adrenal axis and central Fos activation in rats after acute systemic endotoxin exposure. *Neuroscience* 156, 1093–1102. <https://doi.org/10.1016/j.neuroscience.2008.08.011>.
  44. Chuluyan, H.E., Saphier, D., Rohn, W.M., and Dunn, A.J. (1992). Noradrenergic innervation of the hypothalamus participates in adrenocortical responses to interleukin-1. *Neuroendocrinology* 56, 106–111. <https://doi.org/10.1159/000126215>.
  45. Ericsson, A., Kovács, K.J., and Sawchenko, P.E. (1994). A functional anatomical analysis of central pathways subserving the effects of interleukin-1 on stress-related neuroendocrine neurons. *J. Neurosci.* 14, 897–913. <https://doi.org/10.1523/JNEUROSCI.14-02-00897.1994>.
  46. Hermes, S.M., Mitchell, J.L., and Aicher, S.A. (2006). Most neurons in the nucleus tractus solitarius do not send collateral projections to multiple autonomic targets in the rat brain. *Exp. Neurol.* 198, 539–551. <https://doi.org/10.1016/j.expneurol.2005.12.028>.
  47. Pacák, K., and Palkovits, M. (2001). Stressor specificity of central neuroendocrine responses: implications for stress-related disorders. *Endocr. Rev.* 22, 502–548. <https://doi.org/10.1210/edrv.22.4.0436>.
  48. Marvel, F.A., Chen, C.C., Badr, N., Gaykema, R.P., and Goehler, L.E. (2004). Reversible inactivation of the dorsal vagal complex blocks lipopolysaccharide-induced social withdrawal and c-Fos expression in central autonomic nuclei. *Brain Behav. Immun.* 18, 123–134. <https://doi.org/10.1016/j.bbi.2003.09.004>.
  49. Hansen, M.K., O'Connor, K.A., Goehler, L.E., Watkins, L.R., and Maier, S.F. (2001). The contribution of the vagus nerve in interleukin-1 $\beta$ -induced fever is dependent on dose. *Am. J. Physiol. Regul. Integr. Comp. Physiol.* 280, R929–R934. <https://doi.org/10.1152/ajpregu.2001.280.4.R929>.
  50. Liu, X., Nemeth, D.P., McKim, D.B., Zhu, L., DiSabato, D.J., Berdysz, O., Gorantla, G., Oliver, B., Witcher, K.G., Wang, Y., et al. (2019). Cell-type-specific interleukin 1 Receptor 1 signaling in the brain regulates distinct neuroimmune activities. *Immunity* 50, 317–333.e6. <https://doi.org/10.1016/j.immuni.2018.12.012>.
  51. Schiltz, J.C., and Sawchenko, P.E. (2002). Distinct brain vascular cell types manifest inducible cyclooxygenase expression as a function of the strength and nature of immune insults. *J. Neurosci.* 22, 5606–5618. <https://doi.org/10.1523/JNEUROSCI.22-13-05606.2002>.
  52. Zhang, Y.-H., Lu, J., Elmquist, J.K., and Saper, C.B. (2003). Specific roles of cyclooxygenase-1 and cyclooxygenase-2 in lipopolysaccharide-induced fever and Fos expression in rat brain. *J. Comp. Neurol.* 463, 3–12. <https://doi.org/10.1002/cne.10743>.
  53. Elander, L., Engström, L., Ruud, J., Mackerlova, L., Jakobsson, P.J., Engblom, D., Nilsberth, C., and Blomqvist, A. (2009). Inducible prostaglandin E2 synthesis interacts in a temporally supplementary sequence with constitutive prostaglandin-synthesizing enzymes in creating the hypothalamic-pituitary-adrenal axis response to immune challenge. *J. Neurosci.* 29, 1404–1413. <https://doi.org/10.1523/JNEUROSCI.5247-08.2009>.
  54. Parsadaniantz, S.M., Lebeau, A., Duval, P., Grimaldi, B., Terlain, B., and Kerdelluë, B. (2000). Effects of the inhibition of cyclo-oxygenase 1 or 2 or 5-lipoxygenase on the activation of the hypothalamic-pituitary-adrenal axis induced by interleukin-1 $\beta$  in the male Rat. *J. Neuroendocrinol.* 12, 766–773. <https://doi.org/10.1046/j.1365-2826.2000.00517.x>.
  55. Gosselin, D., and Rivest, S. (2008). MyD88 signaling in brain endothelial cells is essential for the neuronal activity and glucocorticoid release during systemic inflammation. *Mol. Psychiatry* 13, 480–497. <https://doi.org/10.1038/sj.mp.4002122>.
  56. Ericsson, A., Arias, C., and Sawchenko, P.E. (1997). Evidence for an intramedullary prostaglandin-dependent mechanism in the activation of stress-related neuroendocrine circuitry by intravenous interleukin-1. *J. Neurosci.* 17, 7166–7179. <https://doi.org/10.1523/JNEUROSCI.17-18-07166.1997>.
  57. Lee, H.Y., Whiteside, M.B., and Herkenham, M. (1998). Area postrema removal abolishes stimulatory effects of intravenous interleukin-1 $\beta$  on hypothalamic-pituitary-adrenal axis activity and c-fos mRNA in the hypothalamic paraventricular nucleus. *Brain Res. Bull.* 46, 495–503. [https://doi.org/10.1016/s0361-9230\(98\)00045-8](https://doi.org/10.1016/s0361-9230(98)00045-8).
  58. Chiu, I.M., von Hehn, C.A., and Woolf, C.J. (2012). Neurogenic inflammation and the peripheral nervous system in host defense and immunopathology. *Nat. Neurosci.* 15, 1063–1067. <https://doi.org/10.1038/nn.3144>.
  59. Taves, M.D., and Ashwell, J.D. (2021). Glucocorticoids in T cell development, differentiation and function. *Nat. Rev. Immunol.* 21, 233–243. <https://doi.org/10.1038/s41577-020-00464-0>.
  60. Kumar, V. (2018). Inflammasomes: Pandora's box for sepsis. *J. Inflamm. Res.* 11, 477–502. <https://doi.org/10.2147/JIR.S178084>.
  61. Martinon, F., Mayor, A., and Tschopp, J. (2009). The inflammasomes: guardians of the body. *Annu. Rev. Immunol.* 27, 229–265. <https://doi.org/10.1146/annurev.immunol.021908.132715>.
  62. Huang, F.-Y., Chan, A.O.-O., Rashid, A., Wong, D.K.-H., Seto, W.-K., Cho, C.-H., Lai, C.-L., and Yuen, M.-F. (2016). Interleukin-1 $\beta$  increases the risk of gastric cancer through induction of aberrant DNA methylation in a mouse model. *Oncol. Lett.* 11, 2919–2924. <https://doi.org/10.3892/ol.2016.4296>.
  63. Krashes, M.J., Koda, S., Ye, C., Rogan, S.C., Adams, A.C., Cusher, D.S., Maratos-Flier, E., Roth, B.L., and Lowell, B.B. (2011). Rapid, reversible activation of AgRP neurons drives feeding behavior in mice. *J. Clin. Invest.* 121, 1424–1428. <https://doi.org/10.1172/JCI46229>.
  64. Fenno, L.E., Mattis, J., Ramakrishnan, C., Hyun, M., Lee, S.Y., He, M., Tucciarone, J., Selimbeyoglu, A., Berndt, A., Grosenick, L., et al. (2014). Targeting cells with single vectors using multiple-feature boolean logic. *Nat. Methods* 11, 763–772. <https://doi.org/10.1038/nmeth.2996>.
  65. Dana, H., Sun, Y., Mohar, B., Hulse, B.K., Kerlin, A.M., Hasseman, J.P., Tsegaye, G., Tsang, A., Wong, A., Patel, R., et al. (2019). High-performance calcium sensors for imaging activity in neuronal populations and microcompartments. *Nat. Methods* 16, 649–657. <https://doi.org/10.1038/s41592-019-0435-6>.
  66. Kohara, K., Pignatelli, M., Rivest, A.J., Jung, H.Y., Kitamura, T., Suh, J., Frank, D., Kajikawa, K., Mise, N., Obata, Y., et al. (2014). Cell type-specific genetic and optogenetic tools reveal hippocampal CA2 circuits. *Nat. Neurosci.* 17, 269–279. <https://doi.org/10.1038/nn.3614>.
  67. Yang, C.F., Chiang, M.C., Gray, D.C., Prabhakaran, M., Alvarado, M., Juntti, S.A., Unger, E.K., Wells, J.A., and Shah, N.M. (2013). Sexually dimorphic neurons in the ventromedial hypothalamus govern mating in both sexes and aggression in males. *Cell* 153, 896–909. <https://doi.org/10.1016/j.cell.2013.04.017>.
  68. Kim, E.J., Jacobs, M.W., Ito-Cole, T., and Callaway, E.M. (2016). Improved monosynaptic neural circuit tracing using engineered rabies virus glycoproteins. *Cell Rep.* 15, 692–699. <https://doi.org/10.1016/j.celrep.2016.03.067>.

## STAR★METHODS

### KEY RESOURCES TABLE

REAGENT or RESOURCE	SOURCE	IDENTIFIER
<b>IHC antibodies</b>		
Mouse $\alpha$ -calcitonin gene-related peptide (CGRP)	Abcam	Ab81887; RRID:AB_1658411
Mouse $\alpha$ -tyrosine hydroxylase (TH)	Immunostar	22941; RRID:AB_572268
Mouse $\alpha$ -protein kinase C-delta (PKC- $\delta$ )	BD Biosciences	610398; RRID:AB_397781
Rabbit $\alpha$ -c-Fos	Abcam	190289; RRID:AB_2737414
Rabbit $\alpha$ -c-Fos	Millipore	ABE457; RRID:AB_2631318
Rabbit $\alpha$ -corticotropin-releasing hormone (CRH)	Abcam	T-4037; RRID:AB_2314240
Rabbit $\alpha$ -GFP	Mol. Probes	A11122; RRID:AB_221569
Guinea Pig $\alpha$ -c-Fos	Synaptic Sys.	226004; RRID:AB_2619946
Guinea Pig $\alpha$ -c-vasopressin (VP)	Peninsula Lab	T5048; RRID:AB_518680
Goat $\alpha$ -mCherry	Sicgen	AB0081; RRID:AB_2333095
Goat $\alpha$ -Cox2	Abcam	Ab23672; RRID:AB_731725
Chicken $\alpha$ -GFP	Millipore	06896; RRID:AB_310288
Icam-1-PE	BD Biosciences	5C11A8; RRID:AB_2721204
Mouse $\alpha$ -FoxP2	Santa Cruz	715-606-151; RRID:AB_2340866
Donkey $\alpha$ -mouse AF647	Jackson IR	711-546-152; RRID:AB_2340619
Donkey $\alpha$ -rabbit AF488	Jackson IR	711-605-152; RRID:AB_2492288
Donkey $\alpha$ -rabbit AF647	Jackson IR	Ab81887; RRID:AB_1658411
Donkey $\alpha$ -guinea pig AF488	Jackson IR	706-545-148; RRID:AB_2340472
Donkey $\alpha$ -goat AF568	Abcam	175704; RRID:AB_2725786
Donkey $\alpha$ -chicken AF488	Jackson IR	703-545-155; RRID:AB_2340375
RNAscope probe – Mm-Pdyn	Biotechne	318771
<b>Flow cytometry antibodies</b>		
CD3-BV711	Biolegend	100349; RRID:AB_2565841
B220-PeCy7	eBiosciences	25-0452-82; RRID:AB_469627
CD4-BV605	Biolegend	100548; RRID:AB_2563054
CD8-BV786	SONY	1103650
CD25-APC	eBiosciences	17-0251-82; RRID:AB_469366
CD44-PE	eBiosciences	12-0441-83
SiglecF-PE	BD Biosciences	553253; RRID:AB_394735
Ly6G-PerCPCy5.5	BD Biosciences	552126; RRID:AB_465665
CD49b-FITC	eBiosciences	560602; RRID:AB_1727563
CD45-PECF594	BD Biosciences	12-5971-82; RRID:AB_466073
Ly6C-BV605	BD Biosciences	562420; RRID:AB_11154401
ckit-APC	eBiosciences	563011; RRID:AB_2737949
CD16/32-PerCPCy5.5	SONY	1106620
CD115-PE	eBiosciences	12-1152-82; RRID:AB_465808
CD19-APCCy7	SONY	1177650
CD43-BV605	BD Biosciences	747726; RRID:AB_2872201
CD24-FITC	BD Biosciences	553261; RRID:AB_394740
BP1-biotin	BD Biosciences	553159; RRID:AB_394671
IgD-BV421	SONY	2688625
IgM-PE	BD Biosciences	553409; RRID:AB_394845

(Continued on next page)

**Continued**

REAGENT or RESOURCE	SOURCE	IDENTIFIER
CD16/CD32 monoclonal blocking antibody	Invitrogen	14-0161-82; RRID:AB_467133
DAPI	Invitrogen	D1306
<b>Bacterial and virus strains</b>		
AAV5-hSyn-DIO-mCherry (AAV-mCherry <sup>flox</sup> )	Bryan Roth lab (ref <sup>63</sup> )	Addgene viral prep # 50449-AAV5
AAV5-hSyn-DIO-hM3D(Gq)-mCherry (AAV-hM3D(Gq)-mCherry <sup>flox</sup> )	Bryan Roth lab (ref <sup>63</sup> )	Addgene viral prep # 44361-AAV5
AAV5-hSyn-DIO-hM4D(Gi)-mCherry (AAV-hM4D(Gi)-mCherry <sup>flox</sup> )	Bryan Roth lab (ref <sup>63</sup> )	Addgene viral prep # 44362-AAV5
AAVretro-pgk-Cre (AAVretro-Cre)	Patrick Aebischer lab	Addgene viral prep # 24593-AAVretro
AAV5-CMV-GFP (AAV-GFP)	Translational Vector Core, INSERM UMR1089, Université de Nantes	AAV5-CMV-GFP
AAVretro-Ef1a-mCherry-IRES-Cre (AAVretro-mCherry-IRES-Cre)	Karl Deisseroth lab (ref <sup>64</sup> )	Addgene viral prep # 55632-AAVretro
AAVretro-hSyn-mCherry (AAVretro-mCherry)	Karl Deisseroth lab (ref <sup>64</sup> )	Addgene viral prep # 114472-AAVretro
AAV0-syn-FLEX-jCaMP7f-WPRE (AAV-GCaMP7f <sup>flox</sup> )	Douglas Kim, GENIE Project (ref <sup>65</sup> )	Addgene viral prep # 104492-AAV9
AAV1-hSyn-Cre-WPRE (AAV-Cre)	James M. Wilson	Addgene viral prep # 105553-AAV1
AAVretro-FLEX-tdTomato (AAVretro-TdT <sup>flox</sup> )	Ed Boyden lab	Addgene viral prep # 28306-AAVretro
AAV1-synP-FLEX-splitTVA-B19G (AAV-[G-TVA-GFP] <sup>flox</sup> )	Ian Whickersham lab (ref <sup>66</sup> )	Addgene viral prep # 52473-AAV1
SAD ΔG-mCherry (envA) (Rabies-EnvA-ΔG-mCherry)	Conzelmann's lab	N/A
AAVretro-pEF1a-DIO-FLPo-WPRE (AAVretro-Cre <sup>FRT</sup> )	Li Zhang lab (ref <sup>31</sup> )	Addgene viral prep # 87306-AAVretro
AAV1-EF1a-Flpo (AAV-Flip)	Karl Deisseroth lab (ref <sup>64</sup> )	Addgene viral prep # 55637-AAV1
AAV5-flex-taCasp3-TEVp ([caspase3-mCherry] <sup>flox</sup> )	Nirao Shah lab (ref <sup>67</sup> )	Addgene viral prep # 45580-AAV5
<b>Chemicals, peptides, and recombinant proteins</b>		
Mouse recombinant IL-1β	Biologend	575102
Mouse recombinant TNF-α	Biologend	575204
Mouse recombinant IL-33	Biologend	580502
Mouse recombinant IL-4	Biologend	574302
Leaf anti-mouse IL-4	Biologend	504107
Mouse recombinant IL-13	Biologend	575902
Mouse recombinant IFN-γ	Biologend	575704
Mouse recombinant IL-12	Biologend	577004
E.coli-derived Lipopolysaccharide (LPS)	Sigma	L2654
4-hydroxytamoxifen (4-OHT)	Sigma	H6278
Clozapine-N-oxide (CNO)	Sigma	C0832
Capsaicin	Sigma	M2028
Castor oil	Sigma	259853
Sunflower oil	Sigma	S5007
Shandon Tissue-marking dye	ThermoFisher	10830020
Diclofenac sodium salt	Sigma	D6899
Normal donkey serum	Abcam	7475
Lithium chloride	Sigma	203637
Resiniferatoxin (RTX)	AdipoGen	AG-CN2-0534

(Continued on next page)

Continued		
REAGENT or RESOURCE	SOURCE	IDENTIFIER
Critical commercial assays		
Mouse corticosterone competitive elisa kit	ThermoFischer	EIACORT
Experimental models: Organisms/strains		
C57BL6/J	Charles River	N/A
c-Fos-CreERT <sup>2</sup> or Fos <sup>tm2.1(icre/ERT2)Luo/J</sup>	Jackson Lab (ref <sup>37</sup> )	030323; RRID:IMSR_JAX:030323
NF-κBbs-GFP or FVB.Cg-Tg(HIV-EGFP,luc)8Tsb/J	Jackson Lab	027529; RRID:IMSR_JAX:027529
Vagotomized mice (VGX)	This paper	N/A
Software and algorithms		
Adobe Illustrator 2021	Adobe	N/A
ImageJ 1.53t	Free (NIH)	N/A
ICY software	Free (Pasteur)	N/A
FlowJo V10	BD Biosciences	N/A
PRISM 6 and 8	GraphPad	N/A
Spike2 v9	CED, UK	N/A

## RESOURCE AVAILABILITY

### Lead contact

Further information and requests for resources and reagents should be directed to and will be fulfilled by the lead contact, Gerard Eberl ([gerard.eberl@pasteur.fr](mailto:gerard.eberl@pasteur.fr)).

### Materials availability

This study did not generate new unique reagents.

### Data and code availability

All data reported in this paper will be shared by the lead contact upon request. Any additional information required to reanalyze the data reported in this paper is available from the lead contact upon request. This study did not generate new codes.

## EXPERIMENTAL MODEL AND SUBJECT DETAILS

Experimental procedures were conducted under the strict regulatory compliance of protocols approved by the Committee for Ethics in Animal Experimentation (CETEA) [DAP180080 and DAP200025]. Eight to twelve weeks old wild-type C57BL6/J mice were purchased from Charles River and let to accommodate in our conventional mouse facility for 1-2 weeks before experiments. Only females were used in our experiments (otherwise stated) for more clarity in the amplitude of the response and to avoid dominance effects on the stress response. The transgenic c-Fos-CreERT2 mice (Jackson lab stock #030323) of C57BL/6N genetic background were purchased from Jackson Laboratories and backcrossed twice to C57BL6/J animals. Only c-Fos-CreERT2 heterozygous mice were used in our experiments. NF-κB-GFP (Jackson lab stock #027529, 100% FVB genetic background) transgenic mice were used as homozygous and kept under the same genetic background. Before all experiments, mice were habituated to handling and to sham intraperitoneal injections at least twice.

## METHOD DETAILS

### Cytokine and neuromodulator preparation

For all experiments, when not mentioned otherwise, IL-1β was injected intraperitoneally at 25 or 50 μg/kg, depending on the batch of cytokine, which can lead to a variation in the CS response as shown in Figure 2C and its repeat in S2B. For other cytokines or endotoxins, the following doses were used: TNF-α, 100 μg/kg; IL-33, 250 μg/kg; IL-13, 250 μg/kg; IFN-γ, 250 μg/kg; IL-12, 250 μg/kg; LPS, 500 μg/kg. To be active, IL-4 (2 μg, 100 μg/kg) was premixed to anti-IL-4 (10 μg, 500 μg/kg) 1 min before dilution with saline (Finkelmann et al., 1993). All cytokines were diluted in a sterile saline solution.

Capsaicin (Sigma, M2028) was resuspended in 100% DMSO at 10 mg/mL and 10 μg in 30 μL saline were injected subcutaneously into the ear pinnae or skin of the back (final 3% DMSO, 0.5 mg/kg) or intraperitoneally at 10 μg/kg or 50 μg/kg.



### Drug preparation

Clozapine N-oxide (Sigma, C0832) was dissolved in DMSO at 50mg/mL and stored at -20°C until use. The day of the experiment, CNO was diluted into saline and injected intraperitoneally at 1mg/kg (2% DMSO final).

4-hydroxytamoxifen (Sigma, H6278) was dissolved in ethanol at 10mg/mL by shaking at 37°C for 30 min and stored at -20°C until use. The day of the experiment, aliquots were shaken at 37°C for 30 min to resuspend 4-OHT precipitates. The 4-OHT was added to the same volume of a 1:4 mixture of castor oil (Sigma, 259853):sunflower oil (Sigma, S5007) and vigorously shaken for 5 minutes. The ethanol was then evaporated by vacuum centrifugation for 2-3 hours. The final 10mg/mL was further diluted in oil to obtain a 2mg/mL solution, injected intraperitoneally at 20mg/kg.

Diclofenac (Sigma, D6899) was dissolved in water at 15mg/mL by shaking for 15min at RT, prior to each experiment. The following stock was further diluted in saline for injection intraperitoneally at 5mg/kg.

Lithium chloride (Sigma, 203637) was dissolved in water (0.3M) and injected intraperitoneally at 120mg/kg (10ml/kg).

Resiniferatoxin (RTX; Adipogen) was dissolved in 100% DMSO (stock solution at 1mg/ml) and final escalating doses of RTX were prepared in saline solution containing 1% DMSO and 1% Kolliphor (Sigma). For chemical ablation of TRPV1+ neurons, 4 weeks-old C57Bl/6JRJ mice were injected daily on four consecutive days with 3 s.c. injections of increasing doses of RTX (30, 70, 100 µg/kg) and a final i.p. injection (100 µg/kg). Control animals were injected with vehicle (saline + 1% DMSO + 1% Kolliphor).

### Tail-flick antinociception test

To validate the efficiency of the RTX treatment, a tail-flick test was performed on 9 week-old mice using the tail-flick analgesia meter (Columbus Instruments). Briefly, the mouse was gently restrained by hand, and radiant heat was directed onto its tail. Tail flick measurements were taken three times at 60s intervals and averaged. The cutoff time was 30s.

### Blood sampling and corticosterone measurements

For blood analyses, the extreme tip of the mouse's tail was cut and the blood was collected 2-3 times until 10µL of blood were obtained. Importantly for corticosterone measurements, random sampling rotations within the cage were performed to avoid time-dependent biases in corticosterone levels. Throughout the course of the experiment, mice were always kept in their homecage in the same room, and stressful cues such as noise were reduced to the minimum.

Corticosterone was measured in 5µL plasma, following the manufacturer's instructions (ThermoFisher, EIACORT). Of note, corticosterone is unbound from its carrier proteins using a 1:1 premix with a dissociation reagent. For this reason, we expressed the concentration of corticosterone in the dissociative mix (2-fold dilution compared to the plasma concentration).

### Subdiaphragmatic vagotomy

Mice were anesthetized by intraperitoneal administration of 150mg/kg ketamine and 5mg/kg xylazine. A 10mm skin incision was made left to the linea alba below the diaphragm. The liver and stomach were pulled aside to expose the two vagus nerve trunks, lining along the esophagus. After carefully detaching the vagus nerve from its connective tissue, a small section (~5mm) was excised from both branches. Muscle and skin layers were sutured and post-operative analgesia was maintained for 5 days using 0.1mg/kg buprenorphine.

### Stereotaxic injections of viral vectors

Mice were anesthetized by intraperitoneal administration of 150mg/kg ketamine and 5mg/kg xylazine. Post-operative analgesia was maintained for 5 days using 0.1mg/kg buprenorphine. Mice were placed onto the stereotaxic apparatus and the glass pipet was calibrated based on the lambda/bregma coordinates following Franklin and Paxinos' guidelines (The mouse brain in stereotaxic, 5<sup>th</sup> edition, 2019). A volume of 150nL was bilaterally infused (2nL.s<sup>-1</sup>) at the sites of craniotomy and using the following coordinates (in mm): CeA AP -1.3, ML ± 2.7, DV(Bregma) -4.8; VC AP -7.5, ML ± 0.4, DV(Dura) -3.5; PVN AP -0.7, ML 0.2, DV(Bregma) -4.8; PB AP -4.9, ML ± 1.5 DV(Bregma) -3.7; BST AP +0.15 ML ± 1.1 DV(Bregma) -4.2. Details about the virus injected are presented in the [STAR Methods](#) table. Animals in which post-hoc histological examination showed that viral injection were not in the correct location were excluded from analysis. For transynaptic rabies experiments, the efficiency of the Rabies virus to infect starter neurons was 17.7±3.4%, similarly to previous observations ([Figure 5H](#), up to 25%).<sup>68</sup>

### In vivo calcium recording with fiber photometry

Consecutive to injection of conditional GCaMP7f-expressing AAV vectors into the PB, optic fibers (multimode, Ø 430 µm, NA 0.5, LC zirconia

ferrule) were bilaterally implanted at the site of virus injection and fixed to the

skull with a liquid bonding resin (Superbond, Sun Medical) and dental acrylic (Unifast). Two weeks later, GCaMP7f-expressing neurons were chronically excited with a 473nm solid-state laser (Crystal Lasers) via a 430µm multimode optical fiber (output intensity < 0.1mW) and GFP signal was collected by the same fiber, filtered through a dichroic mirror and filter (MDF-GFP, Thorlabs), and then focused on a NewFocus 2151 Femtowatt photodetector (Newport). Blue light

reflected in the light path was also filtered and measured with a second amplifying

photodetector (PDA36A; Thorlabs). The signals from the two photodetectors were digitized by a digital-to-analog converter (Micro3 1401, CED, UK) at 5000 Hz and then

recorded using Spike2 9 software (CED, UK). For simultaneous dual color photometry, a 473 nm DPSS laser and a 561 nm DPSS laser (output fiber intensity, 0.1 mW; Crystal Lasers) were reflected via a dichroic filter (MD498 GFP, Thorlabs) onto a 488/561 nm dual-edge dichroic beamsplitter (Di01-R488/561, Semrock) and collimated into a 425  $\mu$ m multimode optical fiber (NA, 0.50, Doric Lenses) with a convergent lens ( $f = 30$  mm). The emitted fluorescence was collected in the same fiber and separated by a 510 nm dichroic mirror, filtered ( $525 \pm 19$  nm for GCaMP and  $624 \pm 75$  nm for mCherry) and focused on two respective NewFocus 2151-femtowatt photoreceptors (Newport; DC mode). Animals were progressively habituated to the fiber optic patch cord (Doric Lenses, Quebec) and to the connection procedure 3–5 days before the recording session. A typical recording session included 4 h of baseline measurements (starting at zeitgeber time 1), followed by 6 h post-saline injections and another 6 h post-IL-1 $\beta$ . Recordings with low GCaMP baseline fluorescence signals (mean fluorescence < 0.15 mV and/or spontaneous events in  $\Delta F/F < 1\%$ ) or displaying movement/laser artefacts were discarded from the analysis. For the recording during foot shock, mice were individually placed in a homemade electrifiable grid floor Plexiglas arena (20x15 cm) connected to a constant-current (DC) shock generator (Supertech instruments, Switzerland) triggered by the DAC acquisition (Micro3 1401, CED, UK). For analysis of fluorescence signals, the raw GCaMP7f signal traces from each detector were first smoothed (smoothing window = 1 s) and then used to calculate a continuous  $\Delta F/F$ , defined as  $[F(t) - F_o(t)]/F_o(t)$ , where  $F(t)$  is the raw smoothed GCaMP7f signal trace and  $F_o(t)$  is the mean fluorescence intensity within sliding window (20 s) centered on time  $t$ . To extract spontaneous population fluorescence transient with the same threshold in all individuals independently of their  $\Delta F/F$  amplitude, we calculated a z-score-normalized fluorescence  $F'$ , defined as  $[F(t) - F_o(t)]/\sigma(t)$ , where  $\sigma(t)$  is the standard deviation of the  $\Delta F/F$  signal in a sliding window (100 s) centered on time  $t$ . From this z-score-normalized fluorescence  $F'$ , all the events above 3SD were automatically extracted with custom scripts (Spike2, CED, UK; minimum time interval, 10 s) and the peak amplitude of each event was then extracted from the  $\Delta F/F$  signal. The frequency of the sorted spontaneous events was then reported as the number of events per unit of time (20 min) and normalized to the 2-hour baseline activity before treatment (baseline set to 1). For the mean fluorescence analysis, the raw GCaMP7f signal traces were downsampled (0.5 Hz), smoothed (100 s), averaged every 20 minutes and normalized to the 2-hour baseline mean fluorescence before treatment. Motion artifacts were examined using simultaneous dual color photometry of the calcium-sensitive fluorescent reporter GCaMP7f and the calcium-insensitive fluorescent report mCherry. mCherry traces were qualitatively different from GCaMP, with no noticeable fluctuation with the same laser power configuration (peak mCherry  $\Delta F/F < 2\%$ ) and no systematic correlated events on both channels. Animals in which post-hoc histological examination showed that viral injection or implanted optic fiber were not in the correct location were excluded from analysis. Investigators were not blinded to the group identity, but automatic analysis routines were performed with the same script executed for each experimental group.

### Histology and immunostaining

Mice were perfused transcardially with phosphate buffered saline (PBS), 2 min, followed by 4% paraformaldehyde (PFA), 7–10 min. Dissected brains were post-fixed for 2 hours in PFA, rinsed twice in PBS for 6 h and placed in PBS containing 30% sucrose for at least 24 h. 60  $\mu$ m-floating sections were obtained using a freezing microtome (Leica). For brain hemisphere identification, a black tissue marking dye (ThermoFisher, 10830020) was used to detect the right hemisphere on brain sections. The sections of interest were stored in PBS with 0.01% azide until use.

For immunostaining, brain sections were first permeabilized/blocked with a 0.2% Triton X-100 (PBS-Triton)/10% Normal Donkey Serum (NDS, Abcam, Ab7475) solution for 2 h at room temperature. Primary antibodies were diluted in PBS-Triton containing 3% NDS and 1% bovine serum albumin (BSA) and incubated with brain sections for 48–72 h at 4°C. The following dilutions of antibodies were used:  $\alpha$ -CGRP (1:500),  $\alpha$ -TH (1:4000),  $\alpha$ -PKC- $\delta$  (1:1000),  $\alpha$ -c-Fos (1:2000),  $\alpha$ -CRH (1:500),  $\alpha$ -VP (1:2000),  $\alpha$ -RFP (1:2000),  $\alpha$ -GFP (1:2000),  $\alpha$ -cox2 (1:100),  $\alpha$ -icam-PE (1:500). Brain sections were rinsed twice with PBS and further stained with Alexa-conjugated  $\alpha$ -mouse,  $\alpha$ -rabbit,  $\alpha$ -guinea pig,  $\alpha$ -goat,  $\alpha$ -chicken secondary antibodies (1:1000) in PBS-Triton 2% NDS for 2 h at room temperature. DAPI stain (1:10000, ThermoFisher, D1306) was used in the first of three PBS washes before sections were mounted on slides with FluoroMount-G (Interchim). All steps were carried under constant agitation.

For in situ hybridization coupled to IHC, manual RNAscope® was performed using mouse probes (ACD Bio) against pDyn (Mm-Pdyn, #318771). 16  $\mu$ m sections of brain tissue were obtained from PFA-fixed and cryoprotected brain tissue sectioned on a cryostat. The sections obtained were attached on Superfrost Plus Adhesion Slides (Thermo Fisher), dried for 15 min at RT before storage at -80°C. After air dry and complete desiccation in successive increasing concentration of alcohol, slides were pre-treated by serial submersion in PBS and hydrogen peroxide for 10 min at RT. An hydrophobic barrier was created using Hydrophobic Barrier Pen (Vector). Following 15 minutes protease treatment at 40°C (ACDBioTechne), probe hybridization was achieved by incubation of mRNA target probes for 2 h at 40°C (Hybe oven). The signal was then amplified using TSA amplification from RNAscope Multiplex Fluorescent v2 assay (ACDBioTechne) and revealed with Opal 520 (Akoya Biosciences). Each incubation step was followed by two 2 min washes using RNAscope washing buffer. Following 15 min rinse in PBS, the slices were processed for immunofluorescence against RFP. For immunostaining, slides were first permeabilized/blocked with a 0.2% Triton X-100 (PBS-Triton)/4% BSA solution for 30 minutes at room temperature. Primary antibodies were diluted in PBS-Triton containing 4% BSA and incubated slides for 24 h at 4°C. Slides were then rinsed twice with PBS and further stained with 594 Alexa-conjugated secondary antibodies (1:1000) in PBS-Triton 4% BSA for 2 h at room temperature. DAPI stain (1:10000) was used in the first of three PBS washes before sections were mounted on slides with Mowiol (Calbiochem).

### Image processing and analysis

Images of immunostained brain sections were acquired with an apotome microscope (Zeiss) using the 10X or 20X objectives or with confocal laser-scanning microscope (LSM 900, Zeiss). Z-stack of 10-steps and 30 $\mu$ m-thick were performed and projected as the maximum fluorescence intensity onto a XY plan to obtain the final images. The same parameters of gain and time exposure were used within a given experiment.

Quantification analyses were automatized using the “spot detector” function of ICY software for the following staining: c-Fos, FoxP2, DAPI. For co-expression analyses, c-Fos, DAPI and FoxP2 were detected by ICY while markers such as CGRP, PKC- $\delta$ , TH, Pdyn, mCherry or GFP were manually counted using the same brightness and contrast parameters in post-acquisition phase. For measurements of immunoreactivity and labeled fluorescence intensity, ROI were manually drawn on FIJI and a fluorescence threshold was applied to remove background before measuring the corresponding labeled area. All images of the same experiment were submitted to the same procedure, and quantification analyses were performed blind.

### Flow cytometry

Organs were harvested and maintained in DMEM medium (Gibco, 31966) on ice until processing. Single-cell suspensions were obtained by grinding the thymus or by flushing out the bone marrow content with a 1mL syringe, and passing the cells through a 70 $\mu$ m filter. Red blood cells were lysed for 1min (bone marrow and thymus) or 5min (blood) with ACK lysis buffer (Gibco, A1049201), followed by blocking unspecific Fc $\gamma$ R binding with anti-CD16/32 for 10 min (Invitrogen, 14-0161-82, not used for bone marrow myeloid cells). Next, cell surface markers were stained for 30min on ice using specific antibody cocktails at the following dilutions: CD3-BV11 (1:100), B220-PeCy7 (1:200), CD4-BV605 (1:200), CD8-BV786 (1:200), CD25-APC (1:200), CD44-PE (1:200), SiglecF-PE (1:200), Ly6G-PerCPy5.5 (1:200), CD49b-FITC (1:200), CD45-PECF594 (1:400), Ly6C-BV605 (1:200), ckit-APC (1:200), CD16/32-PerCPy5.5 (1:200), CD115-PE (1:200), CD19-APCCy7 (1:200), CD43-BV605 (1:50), CD24-FITC (1:200), BP1-biotin (1:100), IgD-BV421 (1:200), IgM-PE (1:200). Dead cells were stained with DAPI (1:10000, Invitrogen, D1306) before acquisition on a BD LSRFortessa. Data analysis was performed on FlowJo V10. Results are representative of one of two independent experiments.

### QUANTIFICATION AND STATISTICAL ANALYSIS

All experimental data were analyzed with the Prism v8 software. Sample normality was tested using the non-parametric Kolmogorov-Smirnov or Shapiro-Wilk statistical tests before analyzing each dataset. The adapted two-sided tests that were used are mentioned within each Figure. All data are expressed as mean $\pm$ SEM and statistical significance is represented by p-values as follow: ns, not significant with  $p>0.05$ ; \*  $p<0.05$ , \*\*  $p<0.01$  and \*\*\*  $p<0.001$ .